Green Chemistry

PAPER

View Article Online
View Journal | View Issue

Cite this: *Green Chem.*, 2026, **28**, 4225

Lignin as a precursor of a gel electrolyte and salt templated carbon for sustainable electrochemical capacitors

Amelia Klimek, [a,b,c,d] Lina Amro, [a] Nutthira Pakkang, [d,e] Camélia Matei Ghimbeu, [b,c,f] Elzbieta Frackowiak *[a] and Shiori Suzuki *[d]

Received 17th October 2025,
Accepted 29th January 2026

DOI: 10.1039/d5gc05533d

rsc.li/greenchem

Electrochemical capacitors (ECs) belong to attractive high-power devices; however, their key components often do not meet ecological requirements. Herein, we propose a sustainable EC based on a gel electrolyte and porous carbon, both of which are made from lignosulfonate (LS), a waste-derived technical lignin from wood. First, the uptake ability of the LS-based gel electrolyte was systematically investigated using several concentrations (1–24 m) of aqueous acetate salt solutions containing different cations (Li, Na, and K). An optimized aqueous electrolyte, 5 m KOAc, was selected due to the high ionic conductivity and ion mobility. Next, LS was converted into porous carbons through an environmentally friendly salt templating approach using NaOAc and KOAc, which enabled precise control of the carbon structure and texture. The resulting carbons exhibited predominantly microporous characteristics with specific surface areas ranging from 881 to 1754 $m^2\ g^{-1}$. Raman spectroscopy analysis revealed various degrees of structural disorder (I_{D1}/I_G ranged from 1.37 to 3.00). Finally, ECs were assembled with the LS-based gel electrolyte and salt templated carbons. They achieved a stable operating voltage (1.6 V), reduced self-discharge (loss of ~30% of initial voltage), and a long lifespan (170 h of floating), which is competitive with reference aqueous ECs (loss of ~40% of initial voltage and 120 h of floating). Importantly, the LS gel plays a two-in-one role as an electrolyte and a separator. The lack of electrolyte leakage also ensures safety of the device. To sum up, our study proved that water-soluble LS waste can be transformed into components of green energy storage systems.

Green foundation

1. This work proposes a novel and eco-friendly strategy for effective utilization of lignosulfonate (LS), a waste-derived technical lignin from wood, as a renewable precursor for electrochemical capacitor (EC) components (electrolyte, electrodes, and separator). ECs based on optimized LS-derived components offer a more sustainable, safe and high-performance alternative to conventional aqueous ECs.
2. LS serves as a green precursor for preparing gel electrolytes with high uptake ability, which can reduce the risks of leakage and corrosion processes, thus increasing safety. Thanks to its versatile properties, it also simultaneously serves as a separator, avoiding the use of synthetic membranes. Moreover, this biopolymer was a source of a carbon material prepared through a salt templating approach, which enabled tailoring the carbon structure/texture.
3. In the future, the main feature of the LS-gel electrolyte, *i.e.*, flexibility, could be tested in real devices, expanding its application in wearable electronics.

1 Introduction

Utilization of renewable sources highly depends on unstable weather conditions,[1] necessitating the assistance of energy storage devices, such as electrochemical capacitors (ECs),[2] to store energy when available. High-power density, quick charge/discharge, and long lifespan are the key features of ECs, which are mainly used in the automotive and electronic sectors.[3,4] The growing commercial application of ECs inevitably brings to light important considerations of sustainability as well as further improvement of energy metrics.[5] The term "sustainable" ideally should be applied to a system where every single component is environmentally friendly and can be safely dis-

[a]*Institute of Chemistry and Technical Electrochemistry, Poznan University of Technology, Berdychowo 4, Poznan 60-965, Poland. E-mail: elzbieta.frackowiak@put.poznan.pl*
[b]*Institut de Science des Matériaux de Mulhouse, Université de Haute-Alsace, F-68100 Mulhouse, France*
[c]*Université de Strasbourg, F-67081 Strasbourg, France*
[d]*Research Faculty of Agriculture, Hokkaido University, Kita 9, Nishi 9, Kita-ku, Sapporo 060-8589, Japan. E-mail: suzuki-s@agr.hokudai.ac.jp*
[e]*Department of International Collaborative Program in Sustainable Materials and Technology for Industries between Nagoya University and Chulalongkorn University, Graduate School of Engineering, Nagoya University, Furo-cho, Chikusa-ku, Nagoya 464-8603, Japan*
[f]*Réseau sur le Stockage Electrochimique de l'Energie (RS2E), 80039 Amiens Cedex, France*

posed of or incinerated after use.[5] For meeting the sustainability criteria, the design of ECs should be focused on the modification of the electrolyte and the tailoring of the texture/structure of the electrode material.

The current benchmark for the supercapacitor field is organic-based ECs whose characteristics are summarized in Table S1. These ECs exhibit a wide voltage range (2.5–3.0 V),[6,7] reduced self-discharge,[8] and a long lifespan (1500 h of floating).[7] However, they use flammable, harmful electrolytes (*e.g.*, $(C_2H_5)_4NBF_4$ in acetonitrile) and require inert conditions (Ar or N_2 atmosphere with O_2 and H_2O < 1 ppm) as well as rigorous and time/energy-consuming drying of electrodes.[9] As a greener alternative, neutral-aqueous-based ECs are proposed. Such ECs are characterized by a stable operating voltage up to 1.6 V,[10] a loss of initial voltage by ~40% (self-discharge)[11] and a lifetime up to 120 h of floating.[12] Certainly, organic-based ECs outperform aqueous-based ECs but lack in terms of environmental friendliness. Hence, a lot of research is focused on eco-friendly gel-type electrolytes to increase sustainability. Therefore, the use of commercially available technical lignin, a byproduct of wood pulping, has attracted attention. Lignosulfonate (LS) is one of the traditional technical lignins, produced in the sulfite pulping process,[13] and its market is expected to grow from 1.68 billion USD in 2025 to 2.34 billion USD by 2034.[14] Water solubility is a beneficial characteristic of LS due to the presence of sulfonate groups, which enables facile preparation of energy storage materials as well as contributes to better ionic conductivity.[15]

Gel electrolytes (GEs) are promising functional separators that enhance the charge mobility of ECs and prevent leakage by retaining liquid electrolytes within the polymer network structure, thereby improving safety.[16] Among GEs, hydrogels containing aqueous liquid electrolytes are notably advantageous due to their stability and non-inflammability in contrast to organogels.[17] Furthermore, GEs contribute to reduced leakage current and self-discharge as well as the flexibility of the device,[18,19] although the gel form decreases ionic conductivity and mobility.[20] The main advantages and disadvantages of GEs are summarized in Table S2. Interestingly, the demand for GEs is steadily increasing; recent market analysis forecasts that its global market will grow substantially by 2035 (up to 4.63 billion USD), driven by demand for flexible, safe, and sustainable energy storage devices[21] as shown in Fig. S1.

The existing aqueous GEs for ECs remain nascent and predominantly rely on petroleum-based synthetic polymers, *e.g.*, poly(vinyl alcohol)[22] and poly(methyl methacrylate),[23] although a few alternatives using natural polymers were reported.[24] In the context of life cycle assessment (LCA), climate change potential (CPP) and cumulative energy demand (CED) are crucial indicators to evaluate the sustainability of materials.[25] Table S3 summarizes the examples of polymers used in GEs and their CPP and CED values. Biomass-based polymers exhibit the lowest CPP,[26,27] followed by biopolymers[26,28–30] and petrochemical-based polymers.[25] The classification is not always clear, since biomass is a complex material combining cellulose, hemicellulose, lignin, and other inorganic compounds.[31] Biopolymers, including LS, combine low CCP, which originates from the fact that lignin stores CO_2 during tree growth, and its processing requires fewer fossil inputs.[26] The relatively low CED values of LS arise from the fact that the processing involves only mild conditions (neutralization, purification, or fractionation), unlike the highly energy-intensive production of biomass or petrochemical polymers.[32,33]

In most reported works, aqueous GEs are combined with typical electrolytes, such as H_2SO_4,[34] KOH,[35] and NaCl,[5] exhibiting high water uptake ability, moderate ionic conductivity ($\sim 10^{-3}$ S cm^{-1})[36] and a gravimetric capacitance ranging from 40 F g^{-1} to 129 F g^{-1}.[37,38] Nevertheless, the performance of such aqueous GE-based ECs is limited to only 0.8 V–1.0 V, dominantly because of water splitting.[39] Only a few GEs are combined with a neutral aqueous electrolyte, which can operate up to 1.6 V.[40] Nevertheless, gel characteristics, such as solution uptake and swelling degree, are neglected.[37,40]

In addition to the electrolyte, an equally important component of ECs is the electrode material, whose texture/structure plays a vital role in charge storage.[4] A relatively new approach, called salt templating, is more effective for tailoring the carbon characteristics (*i.e.*, specific surface area, pore size distribution, and degree of structural disorder) *via* selecting the salts and their interaction with carbon cores.[41,42] The C yield of the synthesis salt templated carbon is slightly higher (30%)[43] compared to conventional carbonization combined with CO_2 activation (20–25%).[44,45] Moreover, the environmental friendliness and cost efficiency of the total process are enhanced owing to the use of inorganic salts as templates and water for the removal of templates (>80% of the salt can be recovered after the synthesis).[43] Using a biopolymer as a precursor, a certain amount of residual ash in the final carbon originates from naturally occurring inorganic elements in the precursor.[46] Water washing is not enough to remove such elements; therefore, acidic washing is recommended.

Herein, we synthesized and optimized an EC utilizing water-soluble LS as an original precursor for the main EC components: electrolyte, separator, and electrodes, which is a milestone for the further development of sustainable ECs. For the first time, an LS-based gel electrolyte with optimized solution uptake of acetate salts with different cations (Li, Na, and K) and at several concentrations (1–24 m) was used. Moreover, LS served as a precursor for the preparation of carbon electrodes through the salt templating approach. The resultant EC based on the LS-derived gel electrolyte and salt templated carbon improved the EC energetic metrics. Nonetheless, employing an LS gel obviates the necessity for a separator, hence improving safety and environmental impact.

2 Experimental

2.1 Materials

Purified lignosulfonate (LS) was kindly supplied by Nippon Paper Industries Co. Ltd, purity: 92%, sulfonate content: 6.6%,

relative molar mass: 33 600 Da, and used without further purification. Poly(ethylene glycol) diglycidyl ether (PEGDGE, repeating unit of PEO = 22) (Denacol EX-861) was provided by Nagase ChemteX Corp. Even though PEG (polyethylene glycol) is currently produced from bioethanol, the epoxidation processing (PEGDGE) is still challenging in terms of eco-friendliness. Lithium acetate (LiOAc), sodium acetate (NaOAc), and potassium acetate (KOAc) (≥99%) were purchased from Sigma-Aldrich, while potassium hydroxide (KOH, ≥85%) was obtained from POCH. The commercially available carbon YP80F (Kuraray) was used as a reference carbon. The binder PTFE (60 wt% solution in H_2O) was provided by Sigma-Aldrich, while conductive carbon black (C65) was provided by Imerys. A glass fiber GF-A separator was purchased from Whatman.

2.2 Preparation of the LS-derived GE (LSGE)

LS (3 g) and PEGDGE (1.2 g) were dissolved in distilled water (5.4 mL) at RT (25 °C). The ratio between LS and PEGDGE was 1 : 0.4 (w/w). The schematic illustration of the preparation of the LS-derived GE is shown in Fig. 1. The molar ratio of epoxy groups in PEGDGE to total hydroxy groups in LS was determined *via* ^{31}P NMR and was consistently maintained at 0.17 $mmol_{epoxy}/mmol_{OHtotal\text{-}LS}$ (Tables S4 and S5). After stirring for 24 h, 10 M KOH (0.6 mL) was added dropwise to the solution and stirred for 5 min. The resultant mixture was degassed using a centrifuge (15 min, 8000 rpm) and then transferred in between two glass plates with 200 μm thick PTFE strips as a frame. After standing at RT for 24 h, the gel thin film was peeled off the glass plates and repeatedly washed with distilled water (minimum 3 times every 24 h). The water present in the gel structure was exchanged into the selected acetate aqueous solution (LiOAc, NaOAc, and KOAc) by changing the solution into a fresh one 3 times every 24 h to yield LSGE. Each product was labelled indicating the acetate solution used and its molal concentration (1–24 mol $(kg\ H_2O)^{-1}$); *e.g.*, LS-5 m KOAc.

2.3 Preparation of LS-based salt templated carbon (CLS)

LS (50 g) as a carbon precursor was dissolved in distilled water (250 mL) and stirred overnight at RT. The selected acetate salt (NaOAc or KOAc) (25 g) was then added to the solution and further stirred overnight at RT. The scheme of the LS-based salt templated carbon preparation is shown in Fig. 1. Additionally, a mixture of two acetate salts, NaOAc (25 g) and KOAc (25 g), was used as well. The resultant mixture was dried in an oven at 80 °C for a minimum of 5 days. The LS and template salt mixture was then carbonized at 900 °C for 1 h in N_2 flow (heating degree 3 °C min^{-1}) to obtain salt templated carbon. A slow heating rate resulted in rather slow generation of volatile compounds, and hence, less disturbance of the molecular orientation in the material.[47] The salt was removed by washing with distilled water. Furthermore, the obtained material was washed with 0.1 M HCl (500 mL) solution to remove ash, and then distilled water, to maintain a pH of 7. To reduce the harmful impact of acidic washing, HCl was diluted and wastewater treatment, including neutralization of HCl to NaCl, was realized. Finally, the purified carbon was dried at 80 °C overnight and subsequently ground in a mortar. The prepared carbons were labeled to distinguish the salt used, *i.e.*, CLS-NaOAc, CLS-KOAc, and CLS-NaKOAc. The C yield of the synthesis of the LS salt templated carbons ranged from 16% for CLS-KOAc, 24% for CLS-NaKOAc to 20% for CLS-NaOAc in line with other works and commercial carbons. The C yield depends on the salt type, *e.g.*, KOAc leads to lower yields than NaOAc because potassium promotes gasification. Additionally, one LS-derived carbon was prepared without using a salt template. In that particular case, the steam activation process was performed during 1 h hold at 900 °C by introducing steam at a rate of 10 mL h^{-1}. The steam activated carbon was labelled as CLS-SA.

2.4 Physicochemical characterization

A conductivity meter and a pH meter (Mettler Toledo) were used to measure the conductivity and pH of the prepared elec-

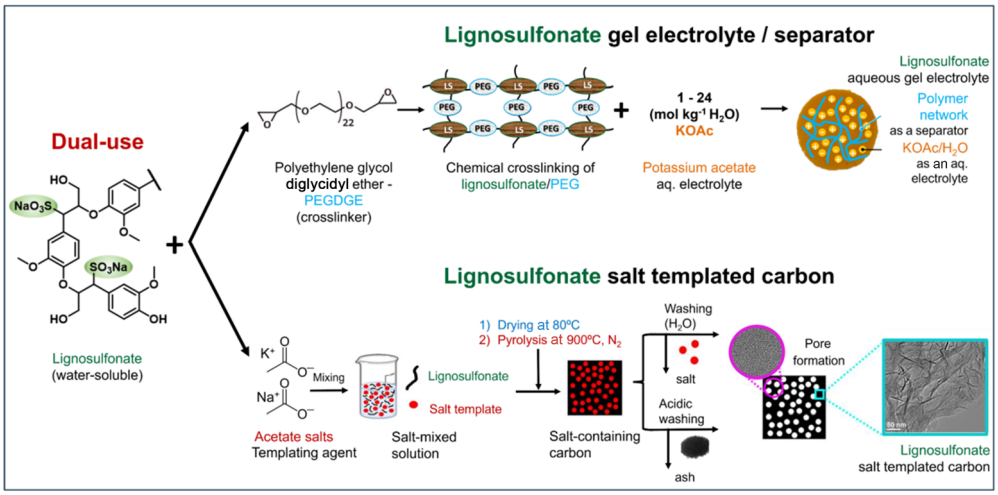

Fig. 1 Schematic illustration of the preparation of an LS-based gel electrolyte and salt templated carbon.

trolytes at RT. The viscosity of the electrolytes was measured using a Brookfield DV2T viscometer at RT. A PerkinElmer FTIR spectrophotometer was used to record the electrolyte absorption spectra (resolution of 4 cm^{-1}). Solution uptake of the LSGEs was calculated according to the mass change measured by weighing the gel film before and after exchange of water into the selected acetate solution. The swelling degree of LSGEs was determined based on the diameter variation before and after the acetate solution exchange. Electrochemical impedance spectroscopy (EIS) was used for conductivity measurement of the LSGEs. High resolution transmission electron microscopy (HRTEM) observation was performed using a JEOL ARM-200F operating at 200 kV to investigate the morphology of the carbons. Raman spectra were acquired using a laser with λ = 532 nm and a power of 3 mW (Thermo Scientific DXR-Raman microscope). The average Raman spectra were deconvoluted into four peaks utilizing the Lorentzian fitting function.[48] The I_{D1}/I_G ratio was determined using peak integrated areas. Nitrogen sorption measurements were conducted using Micromeritics ASAP 2460 apparatus at 77 K on LS-carbons prior to degassing at 300 °C for 24 h. The specific surface area (SSA) was determined using DFT and BET models based on the linear relationship of relative pressures from 0.01 to 0.05. The pore size distribution was obtained using a 2D-NLDFT heterogeneous surface model for carbon materials (SAIEUS, Micromeritics). The slit pores and adsorption branch were considered. Elemental analysis (Thermo Scientific FlashSmart Elemental Analyser, USA) was performed to measure the wt% content of C, H, N, S and O in the carbons.

2.5 Electrochemical characterization

Electrodes were prepared by mixing 90 wt% of the selected LS-derived carbon or commercial carbon, 5 wt% of PTFE as a binder, and 5 wt% of carbon black (C65) to improve the conductivity. These components were combined in a mortar using isopropanol to achieve a uniform paste. Then, the paste was subsequently press-rolled to obtain a thin film of 200 μm in a calendaring machine. The film was cut into disc electrodes with 10 mm diameter (mass loading: ~10 mg) and then dried in an oven at 80 °C for 24 h. The LSGE was cut into 12 mm discs (thickness: ~200 μm). The prepared LS-electrodes and GE were placed in symmetric PTFE-based Swagelok systems with stainless steel 316L current collectors. For three electrode measurements, a Hg|Hg_2SO_4 system was used as the reference electrode. The electrochemical performance of LS-based ECs was investigated using a multi-channel potentiostat/galvanostat (VMP3, Biologic). Cyclic voltammetry (CV) was conducted at scanning rates of 1–200 mV s^{-1}, along with galvanostatic charge/discharge (GCD) (0.1–5 A g^{-1}) and EIS (100 kHz–1 mHz). All capacitance values of ECs were calculated per active mass of one electrode utilizing formulas from ref. 49. The lifespan of ECs was determined using the floating procedure,[43] which involves three GCDs (1 A g^{-1}) at the maximum working voltage (1.6 V), followed by a 2 h voltage hold at 1.6 V. Furthermore, the self-discharge technique was employed, followed by a 2 h voltage hold at 1.6 V and the subsequent recording of the open circuit voltage (OCV) over 12 h. During the 2 h voltage hold at 1.6 V, the leakage current was tracked.

3 Results and discussion

3.1 Physicochemical properties of LSGE

A LS-derived hydrogel was synthesized *via* chemical crosslinking of hydroxy groups in LS with a diepoxy-terminated crosslinking agent (PEGDGE) in the presence of an alkali (KOH) to promote efficient reaction,[37,50,51] as shown in Fig. 1.

The 3D microstructure of the LS gel without dehydration was observed using cryogenic-temperature scanning electron microscopy (Cryo SEM).[52] This technique enables the observation of the fully hydrated state, and the inside structure of the gel, while eliminating drying artifacts.[53] Cryo SEM images of our LS show interconnecting hydrogel networks and a macroporous structure with an average pore size of ~11 μm. (Fig. S2a–c). An important mechanical property of hydrogels is compressibility with stress. The LS hydrogel shows an elongation at break value of 13.4% (Fig. S3). Furthermore, compression tests show that the LS gel exhibits a compression modulus (E_{mod}) of 65.9 ± 15.3 kPa. Classical hydrogels, being soft polymeric networks, frequently break down under light compression due to the diminished mobility of chain entanglements and inadequate stress distribution indicated by the E_{mod} of 39–86 kPa.[54] Interestingly, such an LS hydrogel was directly subjected to exchange water for the selected acetate aqueous solutions to prevent significant deformation of the polymer network structure caused by drying.[55]

To quantitatively evaluate the gel uptake capacity and swelling behaviour of LSGEs under different conditions, lithium, sodium, and potassium acetate salts were tested at concentrations of 1, 3, and 5 m. This was conducted to systematically investigate the effects of cation type (Li^+, Na^+, and K^+) and electrolyte concentration on the GE properties. The swelling is seen as effective if the liquid electrolyte is retained within the crosslinked polymer network and results in elevated ionic conductivity values, while simultaneously maintaining the mechanical strength.[56]

The solution uptake and swelling degree changes over the selected electrolytes and concentrations are shown in Fig. 2a. The gel's interconnected porous structure[57] allowed the uptake of acetate solutions, ranging from 0.65 to 0.15 for LiOAc and NaOAc, and from 0.50 to 0.30 for KOAc. However, the solution uptake was decreased with an increase in acetate concentration, regardless of the type of electrolyte. The same tendency was observed for the swelling degree change. Typically, the solution uptake and swelling degree of gels are facilitated by strong affinity between the polymer network and the solvent, as well as the flexibility of the polymer network, yet it can be impeded by the elevated external osmotic pressure resulting from the addition of the salt.[17] The differences in the investigated abilities between the selected cations were less pronounced for KOAc-based GEs, making this solution the most promising.

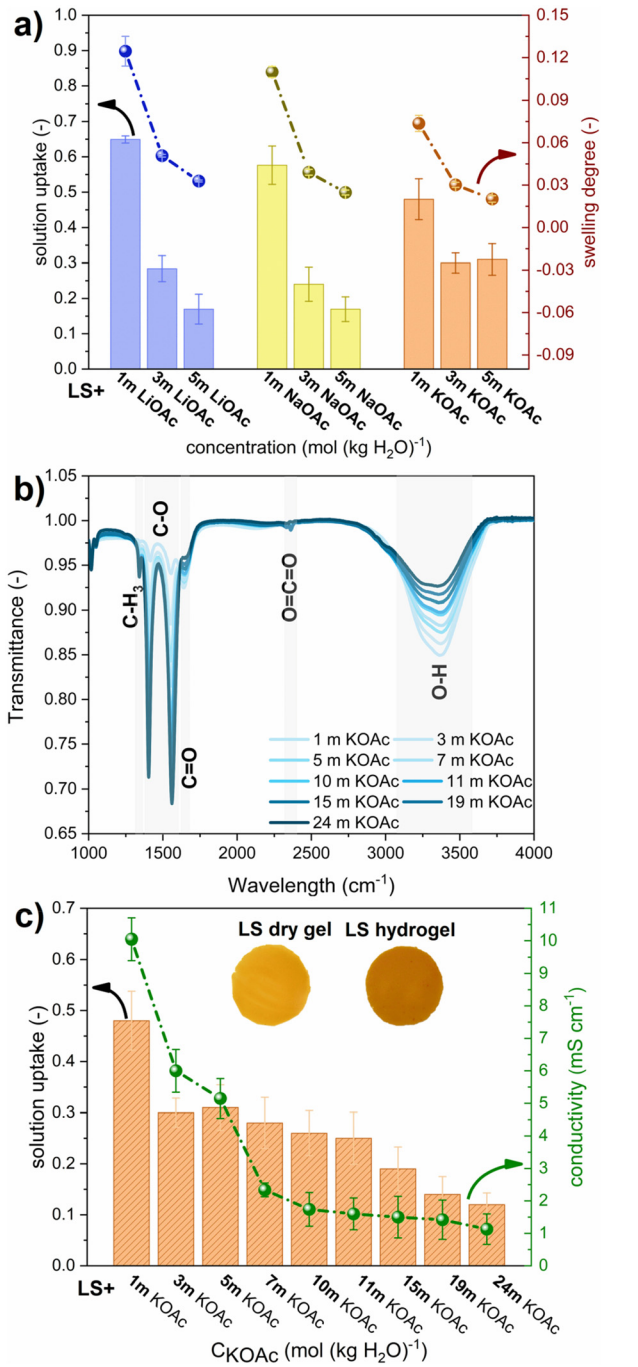

Fig. 2 (a) Solution uptake and swelling degree curve of LSGEs in LiOAc, NaOAc, and KOAc liquid electrolytes at different concentrations (1, 3, and 5 m), (b) FTIR spectra of KOAc at different concentrations (1–24 m), and (c) solution uptake and conductivity of LSGEs in KOAc at different concentrations (1–24 m).

As shown in Fig. S4, the viscosity of LiOAc, NaOAc, and KOAc aqueous solutions increased with higher concentrations. The solution pH was typically alkaline, ranging from 9 to 10 for used acetates, and rather stable within the tested concentrations (Fig. S4). The alkaline condition promotes deprotonation of acidic groups, leading to greater electrostatic repulsion and higher osmotic pressure, thus resulting in higher solution uptake and swelling degree of gels than in acidic medium.[58] Both the solution uptake and swelling degree decreased with increasing alkali acetate concentration, reflecting osmotic pressure reduction and polymer–ion interactions. Notably, the LSGEs in KOAc solution exhibited a smaller performance loss compared to those in LiOAc and NaOAc. This trend can be rationalized by the weaker hydration energy of K^+ ions, which enhances their ability to penetrate and strongly coordinate within the lignosulfonate network.[59]

On the other hand, ionic conductivity was increased up to 5 m only in the case of KOAc, while the increase was visible up to 3 m for LiOAc and NaOAc (Fig. S4). In fact, K^+ has the highest ion mobility, and the lowest hydration enthalpy compared to Li^+ and Na^+ (Table S6), impacting the kinetics of water exchange into the selected acetate. Although high concentrations can reduce the osmotic driving force into the polymeric network, higher ionic conductivity is proportional to ion mobility. Therefore, the solution uptake was increased, confirmed by a nearly equal solution uptake and swelling degree change of 3 m and 5 m KOAc by the gel matrix, even though the viscosity was higher.

The extended study including solution uptake and conductivity of GEs was performed in a wide range of KOAc concentrations (1–24 m), as shown in Table S7, due to the exceptionally high solubility of this salt (256 g per 100 mL at RT).[60] As shown in Fig. S5, the ionic conductivity reached a maximum of 150 mS cm^{-1} at 5 m and then decreased to 40 mS cm^{-1} at 24 m. The pH was strongly alkaline, increasing from 8 to 11 with higher concentrations. The viscosity was increased in the same manner as the pH, ranging from 0.5 to 28 mPa s^{-1}. The FT-IR spectra of KOAc solutions (Fig. 2b) show characteristic bands for KOAc, *i.e.*, $-CH_3$, –C–O, –C═O, and –OH.[61] Moreover, the effect of the change in the concentration was noticeable by the higher intensity/area of the OH band corresponding to the lower KOAc concentrations, containing an increased amount of free water molecules. In the case of <10 m KOAc, the OH band was less broad/intense, due to the formation of a hydrogen bonding network.[62] The GEs with the highest acetate solution uptake was LS-1 m KOAc and showed a high ionic conductivity of 10 mS cm^{-1} at RT (Fig. 2c). The solution uptake and conductivity were decreased with the increase in KOAc concentration (up to 24 m). In general, concentrated aqueous electrolytes higher than 10 m, defined as water-in-salt, are not easily incorporated within the gel network due to the very high viscosity. Among the tested GEs, LS-1 m KOAc exhibited the highest solution uptake, swelling degree and ionic conductivity and could be considered as the most promising. However, the significant amount of existing water in the GE would deteriorate the operating voltage of the EC. Therefore, LS-5 m KOAc with satisfactory characteristics and reduced water content was selected for further electrochemical studies.

3.2 Electrochemical performance of LSGE-based ECs (with commercial carbon-based electrodes)

A stable operating voltage, alongside ionic conductivity, is a crucial parameter for EC electrolytes.[4] To investigate the

electrochemical performance of LSGE, an EC was assembled with electrodes based on commercial porous carbon (YP80F). HRTEM images of this carbon are presented in Fig. S6. These images show a better developed microstructure with short graphene layers that are stacked together in two or three layers. Some isolated (closed) mesopores are seen as well. Moreover, carbon is highly microporous (0.78 $cm^3\ g^{-1}$), with an SSA_{BET} of 2018 $m^2\ g^{-1}$. The isotherm of YP80F is of type I (b), implying also the presence of small mesopores (2–3 nm) corresponding to the mesopore volume (0.24 $cm^3\ g^{-1}$), as shown in Fig. S7 and Table S8. The Raman spectra of YP80F after deconvolution (Fig. S8) proves high disorder of the material, with an I_{D1}/I_G value of 2.50. The stable operating voltage of LS-5 m KOAc was determined by the voltage extension method. It is important that hydrated ion sizes match the average size of micropores of YP80F, assuring effective formation of the electrical double layer (EDL). The triangular shape of GCD curves (Fig. 3a) indicative of EDL performance was noticeable up to 1.6 V. At elevated voltages, the curves exhibited non-linear behavior, including higher ohmic drop, indicating the occurrence of faradaic processes, specifically electrolyte breakdown. To evaluate the electrolyte instability during GCD, the energetic efficiency, a ratio between the integrated values of discharge and charge energy, was assessed.[63] As shown in Fig. 3b, the energetic efficiency remained at 80–85% up to 1.6 V, while it decreased rapidly over 1.7 V. This result suggests that the value of 1.6 V is a stable operating voltage for the LS-5 m KOAc electrolyte. Then, it was further validated by tracking the potential of positive and negative electrodes individually in a three-electrode setup. As shown in Fig. 3c, the positive electrode (E^+) consistently operates beneath the limit of water decomposition, indicated by the oxygen evolution potential, OEP (dashed line). At higher potentials, deterioration of electrodes (carbon oxidation)[10] could take place. In contrast, the negative electrode (E^-) consistently functions beneath the water splitting limit, shown as the hydrogen evolution potential (dashed line). Hydrogen, which is a product of electrolyte decomposition, is electrosorbed by the porous electrode itself.[64] Nonetheless, the GCD curves remained triangular with very high energetic efficiency (Fig. 3a and b), and the positive electrode operated below the OEP (Fig. 3c). Hence, 1.6 V was selected as a stable operating voltage suitable for further advanced electrochemical investigation.

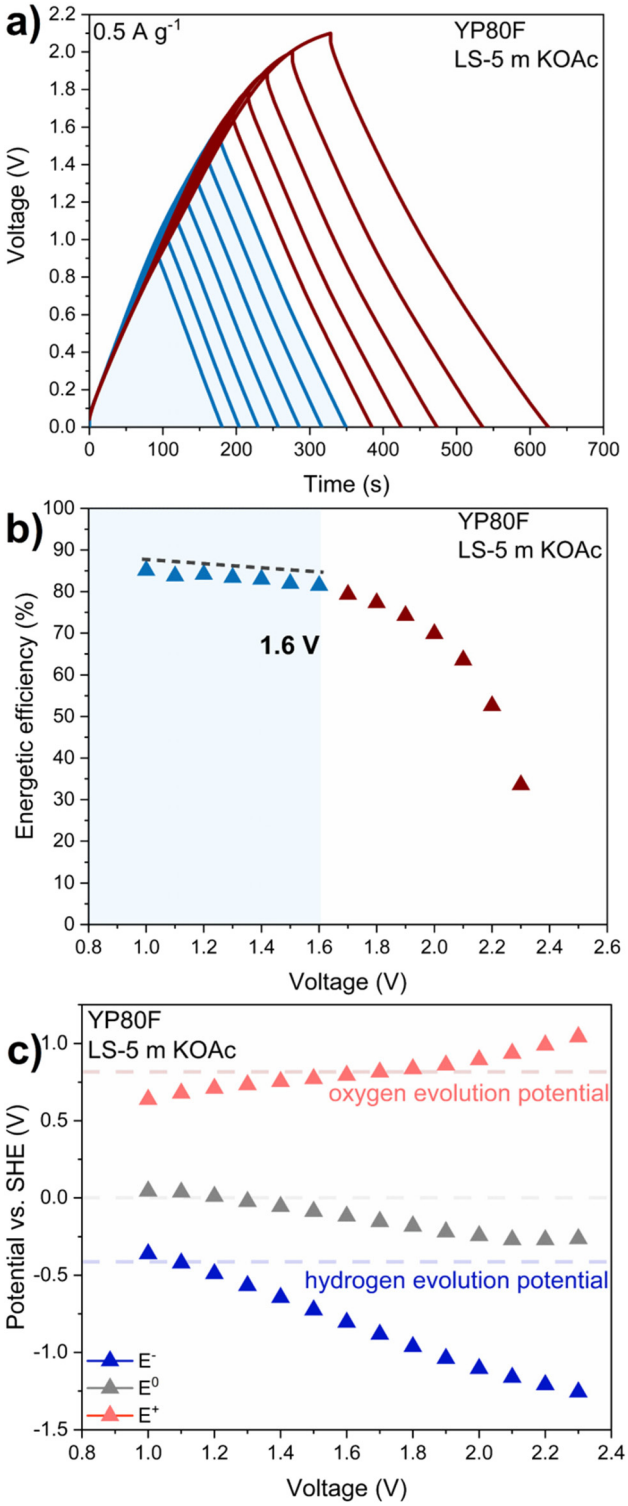

Fig. 3 Preliminary electrochemical performance of YP80F carbon-based ECs operating in the LS-5 m KOAc GE: (a) galvanostatic charge/discharge voltage extension, (b) energetic efficiency *vs.* voltage, and (c) potential of the electrodes (E_0, E^+ and E^-) *vs.* operating voltage.

3.3 Physicochemical characterization of LS-derived carbons

LS-derived carbons (LS-carbon) were prepared by the salt templating approach (Fig. 1), whereas one LS-carbon (CLS-SA) was synthesized by simple carbonization followed by steam activation. In the template method, LS acted as a carbon source, and three different inorganic salts, namely NaOAc and KOAc, and a mixture of both (NaKOAc), were used as templates. Formation of microporosity is possible due to the effect of the salt template (diameter of ions); nevertheless, at the same time, some graphitic domains are formed, influenced by the cation's affinity towards the carbon core[42] (Table S6).

The morphology of the synthesized LS-carbons was observed by HRTEM (Fig. 4a–f and Fig. S9a–f). CLS-SA had a noticeable mixture of dense and mesoporous structures

(Fig. 4a). CLS-NaOAc presented visible graphite domains in addition to more disordered ones while CLS-KOAc showed a disordered structure with no visible porosity or graphitic domains (Fig. 4b and c). In contrast, CLS-NaKOAc presented short stacked graphene layers (2–3 nm, Fig. 4d and e) with obvious mesopores, and long graphitic domains where graphene is stacked in 3–9 layers (Fig. 4f). Carbon's graphitic domains evolve beyond 600 °C, at temperatures higher than the melting points of the salts (325 °C for NaOAc and 292 °C for KOAc), and continue to grow as the temperature rises. This process is significantly influenced by the salt type and its quantity. In this particular case, the mixture of two acetates (NaKOAc) yields the highest level of graphitization, which might be due to its substantial cation–π interactions with the carbon network.[43]

To quantitatively analyze the composition of the carbons utilized in this study, elemental analysis with direct estimation of oxygen was used and the results are presented in Table S9. The highest wt% of the carbon (~95 wt%) as well as the lowest contribution of other elements, including O (~2 wt%), was reported for commercial carbon. In contrast, the LS-carbons present lower wt% of carbon (~85 wt%); however, the negligible presence of N and S was noted as well. The highest amount of O was observed for CLS-KOAc (7.5 wt%), followed

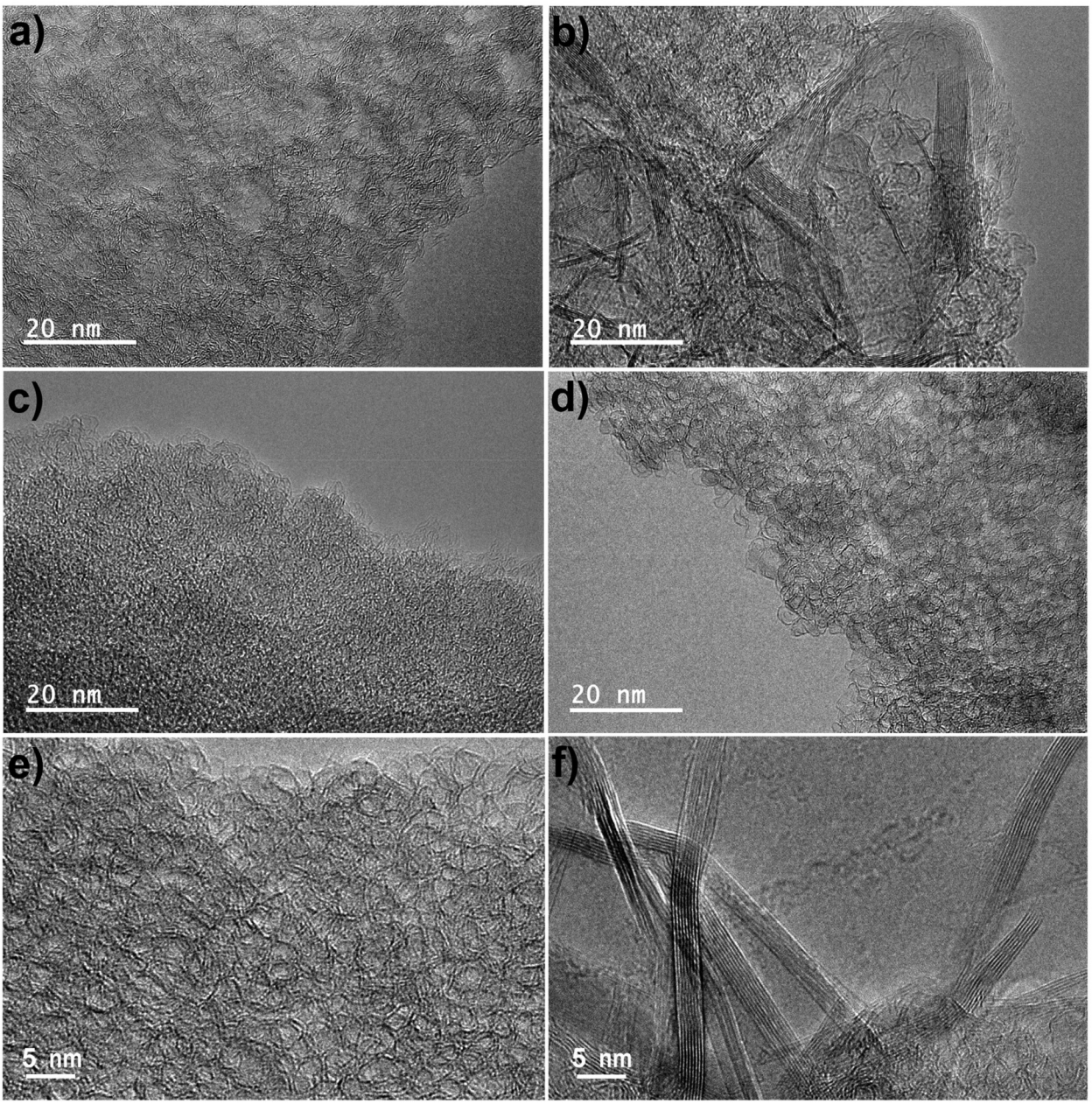

Fig. 4 HRTEM images of LS-carbons: (a) CLS-SA, (b) CLS-NaOAc, (c) CLS-KOAc, and (d–f) CLS-NaKOAc.

by CLS-NaOAc (6.7 wt%), CLS-SA (6 wt%), and CLS-NaKOAc (5 wt%).

The microstructure of LS-carbons was investigated using Raman spectroscopy (Fig. 5). Two principal bands were observed: the disordered-induced band (D) at ~1350 cm^{-1} cm and the first order graphite band (G) at ~1580 cm^{-1}.[65] Additionally, a band in the range of 2500–2800 cm^{-1} denoted as the overtone of the D band (2D) is related to the more ordered structures.[66] As shown in Fig. 5, LS-carbons exhibited well-pronounced D and G bands, but their broadness and height differed. In the cases of CLS-SA, CLS-NaOAc, and CLS-KOAc, the D band was broader than the G band. On the other hand, the G band was intense and narrow only for CLS-NaKOAc, associated with the presence of a 2D band. The ratio of the integrated areas of D and G bands (I_{D1}/I_G) reflects the disorder level of porous carbon materials.[43,48] The I_{D1}/I_G value of CLS-KOAc was 3.00, the highest among LS-carbons, indicating the highest disorder. This value was followed by 2.81 for CLS-NaOAc, 2.61 for CLS-SA, and 1.37 for CLS-NaKOAc. The Raman spectra indicate that LS-carbons have different degrees of disorder, highly disordered for CLS-KOAc, CLS-NaOAc, and CLS-SA, whereas a more ordered structure was observed for CLS-NaKOAc carbon. These results are in agreement with HRTEM analyses.

To investigate the detailed contribution of each band, the deconvolution of D and G bands with a Lorentzian fitting function was performed (Fig. S10). The deconvolution of four peaks revealed two additional peaks, a D_2 band related to a polyene-like structure at the layer edges (associated with the presence of an elevated amount of surface functionalities), and a D_3 band typical of amorphous carbon fractions and functionalities.[43,48] The contribution of the D_2 band (area) was the highest for CLS-NaKOAc, followed by CLS-NaOAc, CLS-SA, and CLS-KOAc. Therefore, CLS-NaKOAc with the lowest degree of disorder shows the highest contribution of surface functionalities at the layer edges in contrast to CLS-KOAc with the highest degree of disorder. The D_3 band area changed in the order from the highest for CLS-KOAc, followed by CLS-NaOAc, CLS-SA, and CLS-NaKOAc. Consequently, the amorphous phase (corresponding to the area of the D_3 band) is the most influential for carbon with the high degree of disorder (CLS-KOAc, CLS-NaOAc, and CLS-SA). These findings based on Raman spectroscopy are supported by the HRTEM observations of LS-carbons (Fig. 4a–d, and Fig. S9), where only CLS-NaKOAc displayed numerous graphitic zones. Porous carbons consist primarily of turbostratic arrangements of graphene-like sheets – aromatic carbon layers that are randomly stacked and twisted, lacking the long-range order found in graphite. These layers form a largely sp^2 hybridized carbon network with defects (topological) and edge sites. The defects in carbon can be defined as vacancies, dislocations, paramagnetic sites, and radicals, as well as surface functional groups. Defects cause uneven distribution of delocalized electrons in the carbon matrix. In disordered carbon, the distance between the graphene domains (d_{002}) is much higher than for graphitic carbons (~0.400 nm for very disordered carbon *vs.* 0.335 nm for graphite).[67] However, it cannot be precisely calculated in the case of salt templated carbons due to the absence of a well-defined d_{002} XRD peak.[43] Therefore, the Tunistra–Koenig relation can be applied on Raman results to calculate La (the size (height) of stacked graphene layers),[65,68] as summarized in Table S10. It is clearly seen that La ranges from 5.58 nm for CLS-KOAc to 12.33 nm for CLS-NaKOAc. Therefore, the graphitic domains formed during carbon preparation are increasing with the cation–π binding energy.[69] It is expected that the crystalline structure of CLS-NaKOAc enhances electron mobility, but more ordered and higher stacked graphitic domains with a reduced distance between the graphene layers are contributing to lower porosity.

The texture of LS-carbons was analyzed by nitrogen sorption at 77 K. Fig. 6a shows the sorption characteristics of all carbons (CLS-NaOAc, CLS-KOAc, CLS-NaKOAc, and CLS-SA). The isotherms are of type I (a) for CLS-KOAc and CLS-NaOAc, indicating their high microporosity and pores with a narrow pore size distribution (<1.0 nm).[42] Regarding CLS-NaKOAc, the isotherm deviates from the perfect type I (a) isotherm, and the shape can be classified as type I (b) isotherm according to the IUPAC.[70] This is specific for materials with a broader pore size, namely larger micropores and/or narrow mesopores. Indeed, the pore size distribution shows in addition the main peak centered at ~0.5 nm, and the appearance of a small peak at ~2–3 nm (Fig. 6b). Differently, CLS-SA presents isotherms of type I at low p/p_0 (<0.2) and of type IV at elevated relative press-

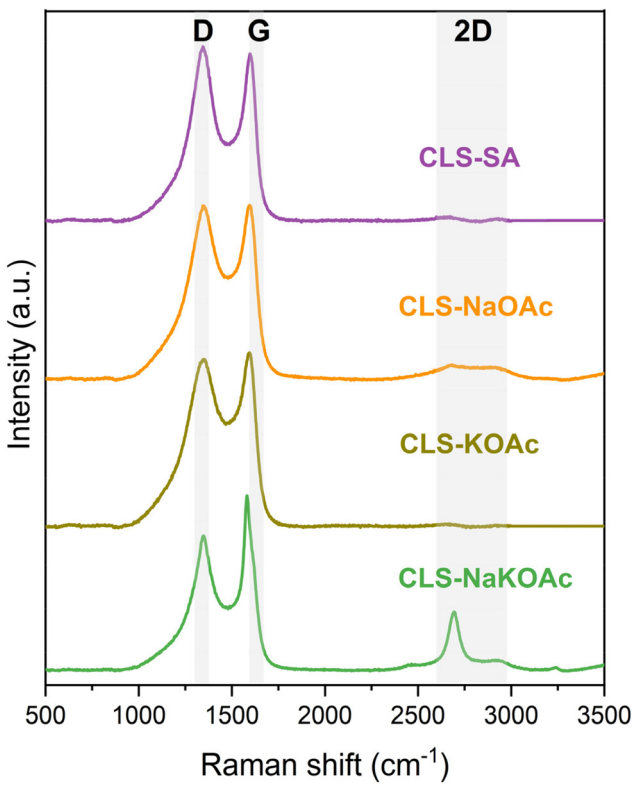

Fig. 5 Raman spectra of all LS-carbons.

ures with an H2 hysteresis loop, characteristic of the presence of both micro- and mesopores. The micropore peak is the narrowest and its maximum is placed at ~1 nm, while the mesopore peak is very broad and ranged between 2 and 8 nm (Fig. 6b). The latter two materials present the highest fraction of mesopores (0.38 $cm^3\ g^{-1}$ for CLS-SA and 0.18 $cm^3\ g^{-1}$ for CLS-NaKOAc, compared to 0.05 $cm^3\ g^{-1}$ for the other materials, Table S11). Therefore, CLS-SA can be considered as a micro/mesoporous material, CLS-NaKOAc is mainly microporous with a minute fraction of small mesopores, while the other materials are rather purely microporous.

The values of S_{BET} of all LS-carbons ranged from 881 $m^2\ g^{-1}$ (CLS-NaOAc) to 1754 $m^2\ g^{-1}$ (CLS-KOAc) as summarized in Tables 1 and S11. Interestingly, Matei Ghimbeu *et al.* reported that templated carbons synthesized using NaCl and KCl had similar S_{BET}.[42] In the case of LS-carbons, the use of NaOAc and KOAc as templates resulted in a significant difference in S_{BET} (Tables 1 and S11) since acetate salts can act as both structural templates and self-activating agents. Also, such a trend can be explained by differences in cation–π binding energy, cation size, and partial graphitization, reducing S_{BET}. Worth mentioning is the fact that the textural and structural characterization was performed on pristine LS-carbons, while for EC testing, LS-carbon based electrodes were used. For the electrodes, the values of S_{BET} and the degree of disorder are slightly lower, equivalent with the wt% of the binder/conductive carbon additive utilized.[69,71]

The *C* values of BET indicate the energy of interaction between the N_2 and the surface of the carbon. Moreover, it is linked to the difference in adsorption energy between the first N_2 adsorbed layer and subsequent layers.[72] The *C* values of 150–200 are associated with micropore filling (strong interaction of the N_2 molecules and carbon surface at low pressures).[70] High *C* values for LS-carbons (from 454 to 839) and for YP80F (332) as shown in Tables S11 and S8 suggest the strongest carbon–N_2 interactions and that the first adsorbed layer is almost complete before the subsequent layers begin to form. Worth mentioning is that the *C* values increase with the increase in oxygen content and total amount of heteroatoms (Fig. S11); therefore, functional groups (especially O-ones) enhance the interaction of N_2 with the carbon surface. The carbons poor in O and rich in C exhibit lower interactions (*i.e.*, YP80F).

Interestingly, the porosity formation mechanisms are different in the case of CLS-SA and salt templated carbons

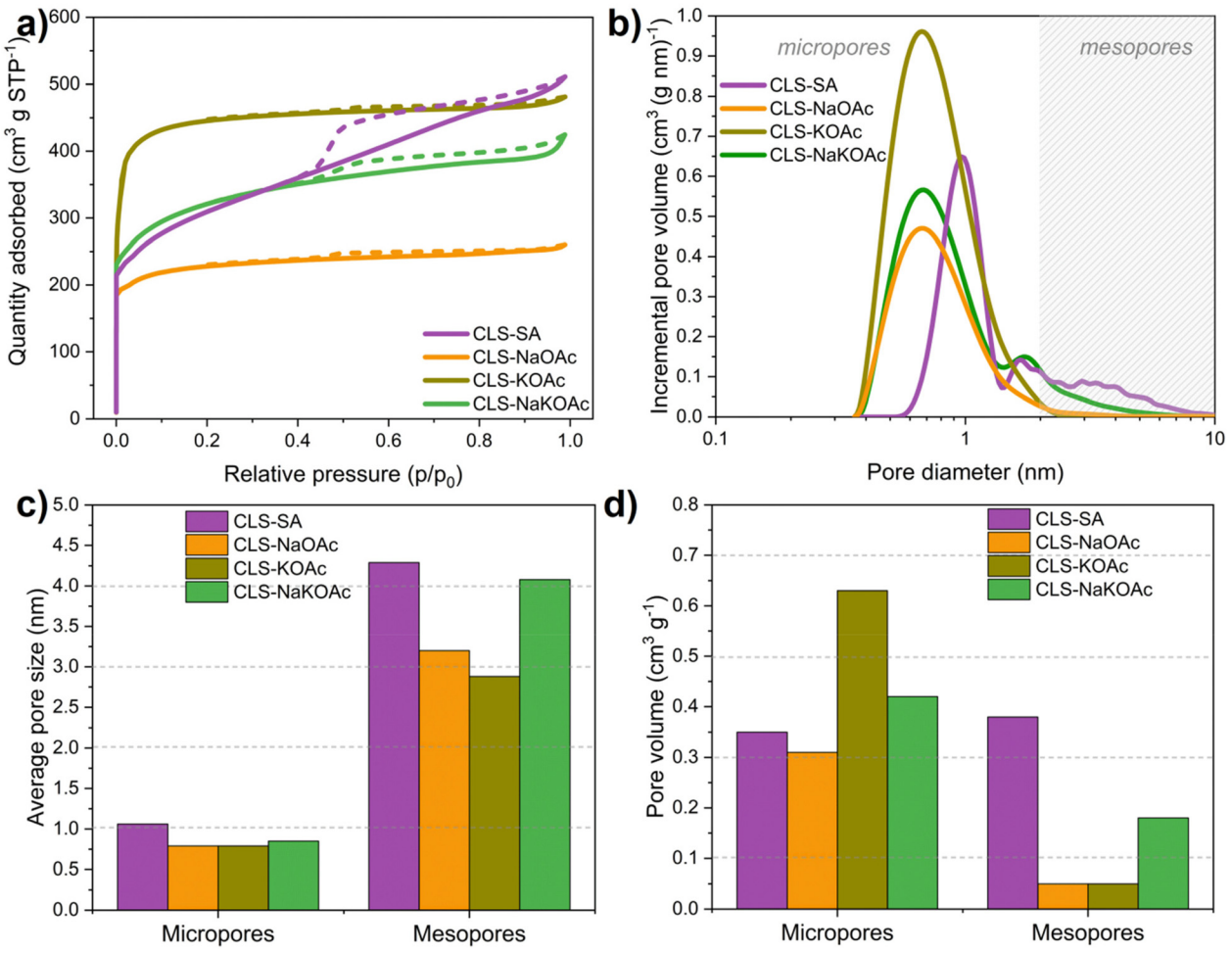

Fig. 6 (a) Nitrogen sorption isotherms at 77 K, (b) pore size distribution, (c) average pore size, and (d) pore volume of LS-carbons.

Table 1 Summary of the physicochemical parameters of LS carbons (S_{BET}, V_{micro}, V_{meso}, $L_{0\ micro}$, O (wt%), I_{D1}/I_G, and La) and the electrochemical performance of LSGE-based ECs (gravimetric capacitance at 0.5 A g^{-1} and floating time)

Carbon	S_{BET}, $m^2\ g^{-1}$	V_{micro}, $cm^3\ g^{-1}$	V_{meso}, $cm^3\ g^{-1}$	$L_{0\ micro}$, nm	O, wt%	I_{D1}/I_G, a.u.	La, nm	Capacitance@0.5 A g^{-1}, F g^{-1}	Floating time, h
CLS-SA	1079	0.35	0.38	1.06	6.0	2.61	6.42	63	58
CLS-NaOAc	881	0.31	0.05	0.79	6.7	2.81	5.96	46	102
CLS-KOAc	1754	0.63	0.05	0.79	7.5	3.00	5.58	82	160
CLS-NaKOAc	1169	0.42	0.18	0.85	5.0	1.37	12.33	52	170

(CLS-KOAc, CLS-NaOAc, and CLS-NaKOAc); therefore, a further discussion is provided. The pore size distribution was determined using two-dimensional nonlocal density functional theory (2D-NLDFT). The advantage of this model is that it eliminates the typical artifacts of the standard homogeneous slit pore model.[73] Fig. 6b illustrates the pore size distribution of LS-carbons, highlighting two regions: up to 2 nm (micropores) and from 2 to 10 nm (mesopores). Micropores are the most helpful in the formation of an EDL, whereas mesopores facilitate the paths for electrolyte ions to access micropores,[74] thereby improving the rate capability.[75] The bar plots in Fig. 6c and d show the average pore size and pore volume of LS-carbons, respectively. The average size of micropores ($L_{0\ micro}$) of LS-carbons did not exceed 1.06 nm, and the size was appropriate for matching the solvated K^+ and OAc^- ions (0.66 and 0.71 nm, respectively), justifying the selection of these carbons for electrochemical capacitor application.

The volume of micropores (V_{micro}) and the volume of mesopores (V_{meso}) are nearly equal for steam activated carbon (CLS-SA). The average size of micropores ($L_{0\ micro}$) of 1.06 nm and the average size of mesopores ($L_{0\ meso}$) of 4.29 nm are shown in Fig. 6c. Similar values were reported for the steam activated carbon from the cellulose fibers as the precursor (S_{BET} = 1018 $m^2\ g^{-1}$, V_{micro} = 0.39 $cm^3\ g^{-1}$).[76] Steam molecules are responsible for a pore-opening process at the surface, thus leading to an increase in surface area. The process of steam activation may lead to the expansion of the pre-existing micropores and the formation of new micropores as steam molecules interact with the carbon matrix.[76,77] Nonetheless, the steam activation process has the tendency to enlarge pores beyond 2 nm, resulting in the formation of mesopores, confirmed by the highest V_{meso} and $L_{0\ meso}$ for CLS-SA among all LS-carbons.

The formation of the texture/structure of the LS salt templated carbons is affected mainly by the interactions of cations with the carbon matrix,[42] the amount of the salt template,[78] the melting point of the salt template[69] and the temperature of the synthesis.[42,78] This was mainly observed when using metal chloride salts. In our case, alkali metal acetates were utilized and we investigated the impact of the different cations in the salt and their quantity on the carbon's texture/structure. Unlike chloride salts, where the salt serves primarily as a template to generate porosity and the cation mainly promotes graphitization, the acetate salts can act as both structural templates and self-activating agents.[79] First, physical templating with acetate salt leads to the development of void spaces and graphitization during carbonization, in a similar manner to chloride salts. During pyrolysis, the molten potassium acetate and the *in situ* formed K_2CO_3/K species can diffuse into the carbon matrix resulting in pore formation and sheet-like morphologies.[80,81] At higher temperatures, chemical activation is induced by acetate salt decomposition *via* the formation of secondary products (*e.g.*, CO_2, K_2O, and K) that react with the carbon framework to widen existing pores or to create new ones. KOAc decomposes at ~440 °C into K_2CO_3, and then into CO_2 and K_2O at ~800 °C. The generated CO_2 etches the carbon framework (activation) to create micropores and mesopores. NaOAc behaves similarly to KOAc with the formation of Na_2CO_3 and CO_2.[79] As for the LS salt templated carbons, the micropore volume (V_{micro}) was the highest for CLS-KOAc (0.63 $cm^3\ g^{-1}$) and the lowest for CLS-NaOAc (0.31 $cm^3\ g^{-1}$). This increase in the micropore fraction is explained by the higher atomic mass/cation size of the alkali metal (K > Na) in the template, in agreement with the results observed on metal chloride salts.[42,69] In contrast, the mesopore volume (V_{meso}) was the same for both carbons (0.05 $cm^3\ g^{-1}$). It proves that the cation type did not influence the mesoporosity but has a significant effect on the microporosity. The binding energy of a cation to the aromatic domains directly impacts the porosity of the carbon; a higher binding energy (Na^+) causes stronger interactions that induce the carbon aromatic sheets to form stacks, thus lowering S_{BET} and V_{micro}, contrary to the cation with a lower binding energy (K^+).[69] On the other hand, there is no difference between the $L_{0\ micro}$ of CLS-NaOAc and CLS-KOAc, since the difference in cation sizes is not significant. However, such a difference is more pronounced considering $L_{0\ meso}$, where the smaller mesopores are reported for CLS-KOAc (2.88 nm) contrary to CLS-NaOAc (3.20 nm).

The quantity of the template salt is influential, and increasing the salt amount in the synthesis can increase the carbon porosity,[79] resulting in higher S_{BET} and V_{micro}.[78] In the cases of CLS-KOAc and CLS-NaOAc, the weight ratio between the carbon precursor and salt was 2 : 1 (w/w), whereas for CLS-NaKOAc, this ratio was 1 : 1 (w/w); hence, the salt quantity was twice higher. Therefore, a significant difference in textural properties between these LS-salt-templated carbons should be observed; however, such results were not observed in this study.

To have a fair comparison of the carbon precursor : salt template ratio effect using the same salt mixture (NaKOAc), a sample with a lower amount of salt (2 : 1, w/w) was prepared. The SSA was lower (752 $m^2\ g^{-1}$ *vs.* 1169 $m^2\ g^{-1}$) and graphitization was less developed (I_{D1}/I_G = 1.80 *vs.* I_{D1}/I_G = 1.37). The V_{micro} of CLS-NaKOAc (0.42 $cm^3\ g^{-1}$) is placed in between

those of CLS-KOAc and CLS-NaOAc. Such a tendency was not observed for V_{meso}, which was the highest reported value (0.18 cm^3 g^{-1}) among the LS salt templated carbons. The development of mesopores when using NaKOAc is induced by a synergetic effect of both salts. A mixture of salts presents a lower melting point than individual salts, enhancing the interaction with the carbon framework and promoting porosity. Excessive etching of the carbon network leads to a decrease of microporosity, micropore widening and the formation of extensive mesopores.[43,75]

Another mechanism that explains the decrease in the micropores and the development of mesopores for CLS-NaKOAc relies on the synergetic effects of NaOAc and KOAc salts, which leads to graphitization of the structure (Fig. 4d, I_{D1}/I_G = 1.37). This is different from CLS-KOAc and CLS-NaOAc, where graphitization does not occur (Fig. 4b and c, $I_{D1}/I_G \sim 3$). The graphitization of CLS-NaKOAc proceeds first by pore closure (lower SSA), approaching the graphene layers and stacking them together (higher La). The short graphene layers stacked in only 2–3 layers are arranged in a concentrical manner and form mesopores (Fig. 4e), while the long and highly stacked graphene layers (Fig. 4f) contribute to the decrease of microporosity and S_{BET}. The graphitization of CLS-NaKOAc can be linked to the salt's interaction with the carbon. The mixed salt presents a lower melting point, strongly interacting with the carbon, leading to graphitization and mesopore formation. This was observed when LiCl was used as a salt template at a pyrolysis temperature (900 °C) exceeding its melting point (~600 °C).[42] Overall, the results allow us to conclude that both the increase of the salt amount and the low melting point of the salt mixture develop the textural properties (micro- and mesopores) and the graphitization level (Table S12).

3.4 Electrochemical performance of green LS-based ECs

Sustainable, LS-based ECs were assembled with LSGE (LS-5 m KOAc) and LS-carbon electrodes to assess the electrochemical performance of the device. The CV and GCD curves of LS-based ECs (Fig. 7a and b) exhibited rectangular and triangular

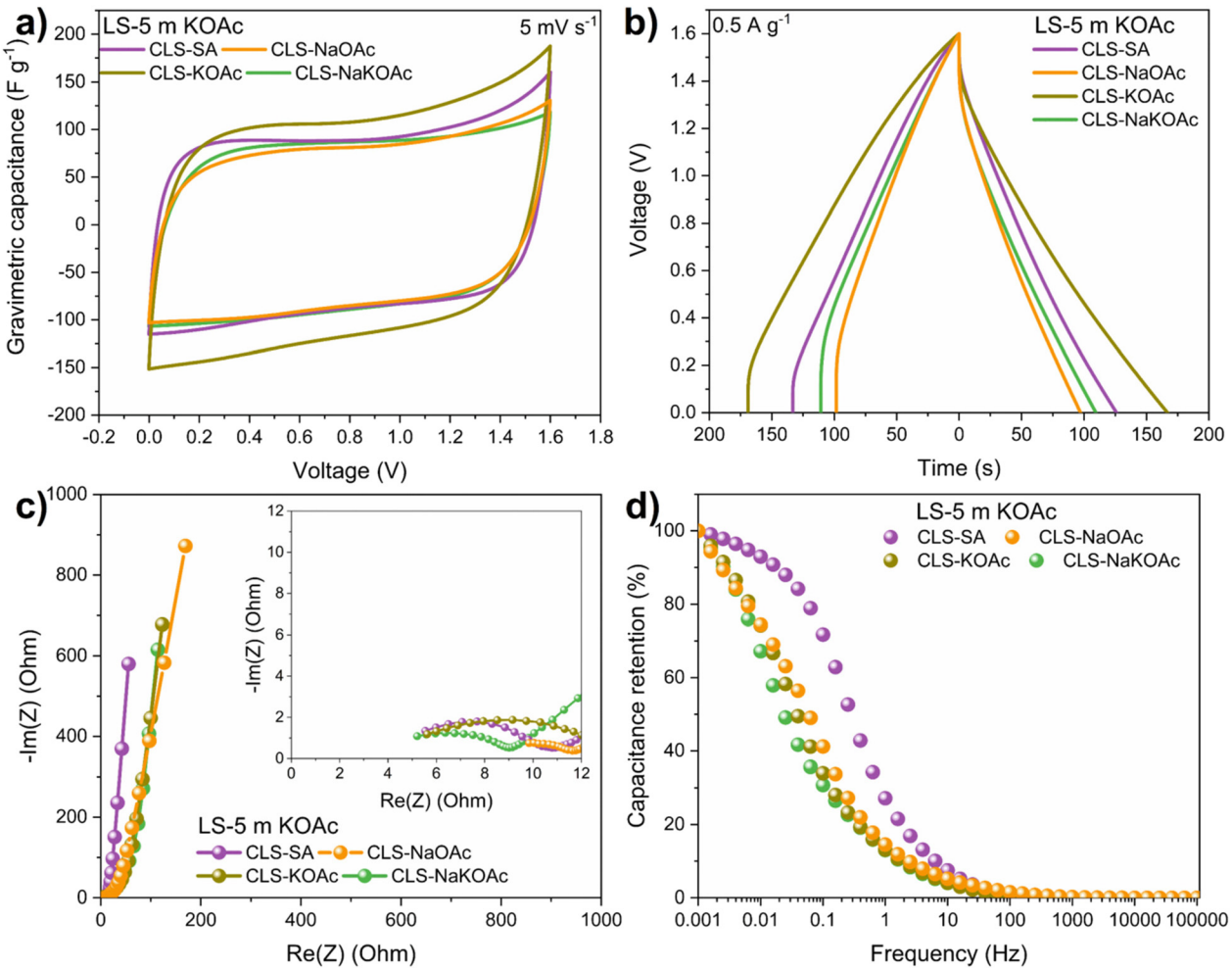

Fig. 7 Electrochemical performance of LS-carbon-based ECs operating in an LS-5 m KOAc GE at 1.6 V: (a) cyclic voltammetry, (b) galvanostatic charge/discharge, (c) Nyquist plot, and (d) capacitance retention *vs.* frequency.

profiles, respectively, within the 1.6 V range, signifying a nearly ideal EDL formation. The gravimetric capacitance was calculated from the integrated area of the galvanostatic discharge curve according to the previous report.[63]

The summary of the physicochemical and electrochemical parameters of LS carbons is shown in Table 1. The gravimetric capacitance at 0.5 A g^{-1} ranged from 46 F g^{-1} to 82 F g^{-1} LS-based ECs (Fig. 7b and Table S13). The highest SSA and I_{D1}/I_G of CLS-KOAc (Table 1) led to the highest capacitance of the EC. In contrast, the smallest SSA of CLS-NaOAc caused the lowest capacitance among LS-based ECs, although the degree of disorder was relatively high. Therefore, the SSA of the carbon material appears to be the most impacting factor for the capacitive performance of ECs.

The charge propagation of LS-based ECs was investigated using EIS. The Nyquist plots (Fig. 7c) were typical of ECs based on activated carbon electrodes.[82] The minor semicircle observed in the high-frequency region is ascribed to the charge transfer impedance related to faradaic reactions. The curve exhibiting a slope in the medium frequency range is generally linked to the diffusion of the electrolyte into the porosity of the electrode material. Finally, the low-frequency region is attained when the entire surface of the electrodes becomes saturated with ions from the electrolyte, resulting in capacitance that is independent of frequency; the recorded value approaches a parallel alignment with the imaginary axis, related to the cell's capacitive behavior.[82,83] The equivalent series resistance (ESR) was determined from the intercept with the real axis at high frequency,[84] and was nearly similar (~5 Ohm) for CLS-KOAc, CLS-NaKOAc, and CLS-SA-based ECs (Fig. 7c). A slightly higher ESR (~9 Ohm) was observed for CLS-NaOAc-based ECs, which could be affected by the cell assembly.[85] Capacitance retention as a function of frequency (Fig. 7d) illustrates better performance in the low frequency range, impacted by the highest mesopore volume for CLS-SA, contrary to the other templated carbons with a higher micropore volume that slows down ion diffusion. Additionally, capacitance retention *vs.* frequency dependence allows the estimation of important EC parameters such as the time constant. The time constants acquired for CLS-based capacitors are placed from 3 s (CLS-SA) to 20 s (CLS-NaKOAc). However, a definitely better value (0.6 s) was obtained for an EC with an LS-gel electrolyte and commercial YP80F carbon (Fig. S12). This means that charge propagation is determined by the electrode and by the gel electrolyte.

The size of ions plays a crucial role in EDL formation. The diameter of the desolvated ions changes from 0.23 nm for K^+ (0.66 nm when solvated) to 0.15 nm for CH_3COO^- (0.71 nm when solvated).[10,86] All ions, even when completely solvated, are supposed to be accommodated within the majority of the pores of the utilized LS-derived carbons ($L_{0\ micro}$ = 0.85–1.06 nm), consequently contributing to the formation of the electrode/electrolyte interface.[5] Insights into the molecular-scale mechanism of charge storage in the EC with the gel electrolyte can be monitored by tracking the behavior of positive and negative electrodes operating in the LS-5 m KOAc GE and carbon (YP80F) (Fig. 3a–c). The formation of a double layer at the interface between the carbon electrode and LS-5 m KOAc GE is evidenced by the nearly perfect, triangular shape of the GCD curve (distinct absence of redox humps up to 1.6 V). Moreover, an energetic efficiency of 82% was noted, confirming good conductivity and low resistance of the system (Fig. 3b). Above 1.6 V, the shape started to deteriorate from the perfect triangular shape. This directly indicates the occurrence of faradaic processes, such as carbon oxidation, current collector corrosion and gradual electrolyte breakdown.[10] The noted faradaic contribution can also be linked to the charge transfer processes taking place among the functional groups found in lignosulfonate, especially with cationic species such as Na^+ and K^+. Lignosulfonate contains hydroxyl (–OH), carboxyl (–COOH), and sulfonate ($=SO_3^{2-}$) functional groups, thereby improving the wettability of the carbon electrode surface. This improvement affects faradaic reactions and supports ion adsorption.[20] Various studies have documented interactions between these functional groups and cations, including K^+ ions derived from the acetate electrolyte.[20,86–88]

Interestingly, information on the charge storage mechanism can also be obtained from the most reliable technique, *i.e.*, galvanostatic charge–discharge. The GCD technique was employed to observe the electrochemical performance of LS-carbons in LSGE-based EC systems (Fig. 7b). The shape of the GCD curve slightly deteriorates from a perfect triangle. Furthermore, lower energetic efficiencies were noted (CLS-SA: 63%, CLS-NaOAc: 46%, CLS-KOAc: 65%, and CLS-NaKOAc: 52%). The noticeable differences in the energetic efficiency values for ECs based on LS-carbons and LSGE can be attributed to the presence of defects and heteroatoms. To quantitatively analyze the composition of the carbons utilized in this study, elemental analysis with direct estimation of oxygen was used and the results are presented in Table S9. The highest wt% of carbon (~95 wt%) as well as the lowest contribution of other elements, including O (~2 wt%), was measured for commercial carbon. In contrast, LS-carbons present a relatively high wt% of carbon (~85 wt%), negligible presence of N and S but a noticeable amount of O (~6 wt%). Therefore, a slight deviation in the GCD shape at 1.6 V and lower values of energetic efficiency (contrary to EC-LSGE-YP80F) can be explained especially by the presence of oxygen functionalities, which reduce the stability of the electrolyte. Carbon rich in oxygen supplies additional charge (*e.g.*, pseudocapacitance from C=O ↔ C–OH)[89] but redox reactions are sluggish/diffusion dependent; hence, EC time constants are higher, and energetic efficiency and power density are lower. In conclusion, the mechanism of charge storage is not purely based on the electrostatic attraction of the ions and subsequent adsorption in the pores; the faradaic reactions related to the presence of oxygen also contribute.

Fig. 8a presents a Ragone plot for LS-based ECs. The energy density reached about ~10 Wh kg^{-1} across a broad power range, indicating high-power characteristics of the device. Additionally, a reference EC based on a 0.5 M CH_3COONa liquid electrolyte was added to the Ragone plot and presents

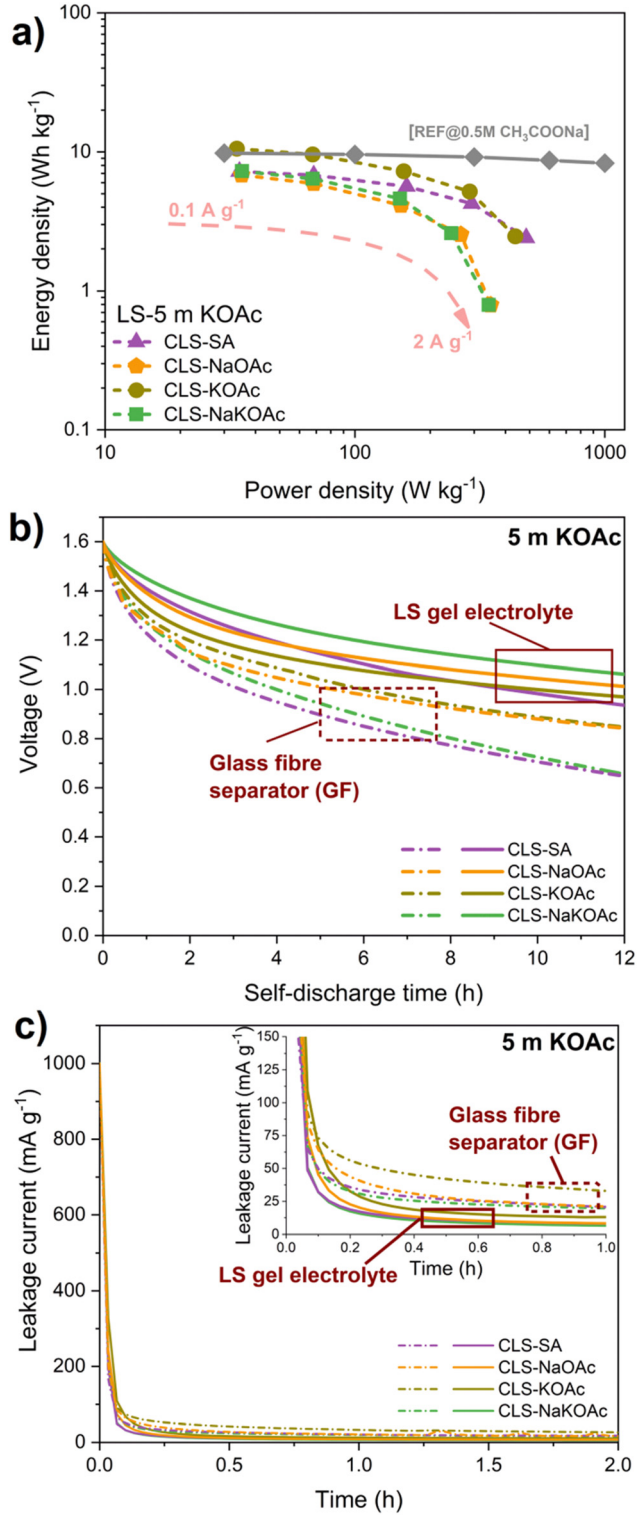

Fig. 8 Electrochemical performance of LS-carbon-based ECs operating in an LS-5 m KOAc (LSGE) or glass fibre separator (GF) with a 5 m KOAc liquid electrolyte at 1.6 V: (a) Ragone plot, (b) self-discharge, and (c) leakage current.

comparable energy metrics with LSGE-based ECs at low current densities. Another important metric of ECs is self-discharge. The spontaneous voltage decline between electrodes under open circuit conditions is referred to as self-discharge.[90] The primary disadvantage of ECs is the relatively rapid self-discharge, due to the charge redistribution in variably shaped pores with liquid electrolytes characterized by high mobility of ions.[91] Rapid self-discharge also reflects leakage current and faradaic reactions.[90] One possible solution to this issue is the use of GEs instead of liquid electrolytes.[40] For this purpose, ECs based on a commonly used glass-fiber separator (GF) and liquid electrolyte (5 m KOAc) were compared to those based on an LSGE (LS-5 m KOAc). As shown in Fig. 8b, the solid-state form of the LSGE considerably influenced the self-discharge of ECs, maintaining a higher voltage (~1 V) for a longer duration compared to the reference system using liquid electrolytes (~0.7 V). Moreover, the self-discharge profiles (Fig. 8b) indicate a diffusion-controlled mechanism, linked to the redistribution of ions within the micropores.[11] Furthermore, the leakage current of LSGE-based ECs decreased in contrast to liquid electrolyte-based ECs (Fig. 8c). This measurement was performed by a 2 h hold of the maximum operating voltage of the system. Under such harsh conditions, the breakdown of the liquid electrolytes occurs faster than for GEs, and generates gases, *i.e.*, CO and CO_2, which shifts the equilibrium of the system, resulting in an increase of the leakage current.[11]

To provide more insights into the operating mechanism, the relationship between the LS-carbon texture/structure and the electrochemical performance was investigated. A strong linear correlation between carbon properties and electrochemical performance ($R^2 > 0.86$ and $R^2 > 0.78$) was observed (Fig. S13a and b), demonstrating that higher S_{BET} and V_{micro} substantially improve gravimetric capacitance. This results from the enhanced accommodation of the electrolyte ions, thereby promoting an EDL capacitive storage mechanism. A similar relationship was already very well investigated and reported elsewhere.[43,75]

The structural defects of carbon arise from *e.g.*, stacking faults, dislocations, multiple vacancies, and edge sites associated with the presence of oxygen surface functionalities.[92] Interestingly, a high coefficient of determination is noted (0.98) when the band D_3 after Raman deconvolution is taken into account (Fig. S13c). Band D_3 originates from the amorphous carbon fraction, comprising functional groups.[43,48] This confirms that Raman spectroscopy and elemental analysis are complementary techniques to provide information on carbon defects.

Linearity is not observed when analyzing the correlation of I_{D1}/I_G with gravimetric capacitance. Typically, such a correlation was observed elsewhere.[43,75,93] This difference may arise from the fact that the synthesized LS carbons are heterogeneous, mainly disordered but with local graphitic domains, as shown in HRTEM images. Also, the relationship of the total oxygen content and gravimetric capacitance deviates from linearity with $R^2 = 0.36$. In our case, the gel electrolyte was utilized, which differs from the conventional aqueous electrolytes and the capacitance values reported for such systems. Both the gel electrolyte and the carbons were synthesized using lignosulfonate (waste from paper production), which has slightly reduced purity.

The next important parameter of ECs is its durability (lifespan). The maximum stable operating voltage (1.6 V) of the LS-5 m KOAc-based EC was set during potentiostatic floating, which is the most credible method for determining the lifespan.[94] Fig. 9 and Fig. S14 show the plots of relative capacitance and relative resistance *vs.* floating time. End-of-life is achieved when 20% decrease in the initial capacitance and/or 100% increase in the initial resistance is recorded.[95] Nevertheless, end-of-life is impacted by the desired application of ECs as well; therefore, achieving just one criterion is satisfactory.[96] As shown in Fig. 9, end-of-life, limited by the initial capacitance decrease, ranged from 58 h (CLS-KOAc-based EC) to 170 h (CLS-NaKOAc-based EC). On the other hand, end-of-life, determined by a relative resistance increase, was reached only for the CLS-NaKOAc-based EC. The degradation of the systems could be ascribed to the decomposition of carbon surface functional groups, water splitting (HER and OER), and carbon corrosion.[97] The most disordered CLS-KOAc (I_{D1}/I_G = 3.00) presenting the highest S_{BET} value (1754 m^2 g^{-1}) demonstrated the shortest floating time, in contrast to the most ordered CLS-NaKOAc (I_{D1}/I_G = 1.37) presenting a lower S_{BET} value (1169 m^2 g^{-1}). Worth mentioning is that the CLS-NaKOAc-based EC showed a rather similar floating time to the CLS-NaOAc-based EC (170 h *vs.* 160 h), although CLS-NaOAc presented a high degree of disorder (2.81) and a low S_{BET} value (881 m^2 g^{-1}).

Importantly, the differences in the end-of-life of ECs depend on the texture and structure of LS-carbons used for electrodes.[43] A higher degree of disorder links with the defect density and reflects the presence of oxygenated functional groups, enhancing wettability and pseudocapacitive contribution. On the other hand, disorder may introduce more electrochemically active sites, resulting in acceleration of parasitic reactions and structural degradation, shortening the lifespan of the device.

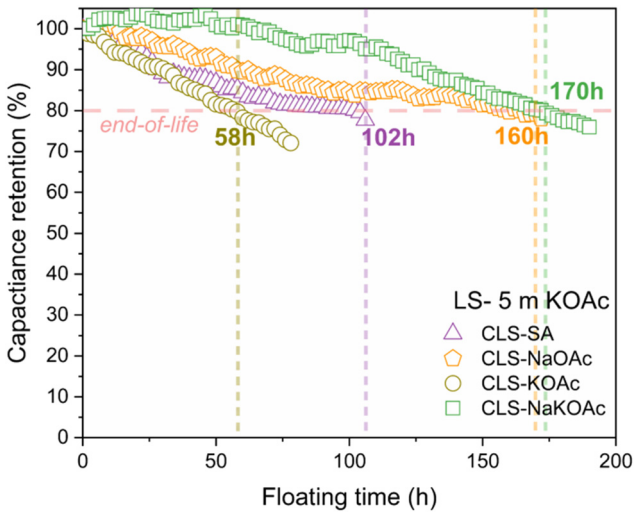

Fig. 9 Relative capacitance *vs.* floating time of LS-carbon-based ECs operating in an LS-5 m KOAc gel electrolyte at 1.6 V.

It is expected that the more ordered structure of CLS-NaKOAc enhances the electron mobility, thus improving the conductivity, resulting in a better lifespan.[43,69] However, more ordered and higher stacked graphitic domains with a reduced distance between the graphene layers and smaller SSAs contribute to a decrease in capacitance. Similarly, a high surface area arising from extensive microporosity increases charge storage but can hinder ion transport, trap solvated ions, and compromise mechanical integrity during long-term performance. In contrast, mesopores create stable ion diffusion paths, which helps to maintain long-term performance,[96] particularly important in gel-based systems where mobility is more limited than in liquid electrolytes. As reported herein, CLS-KOAc, which is the most disordered and porous (the highest I_{D1}/I_G, S_{BET} and V_{micro}), improved the gravimetric capacitance of such a system but shortened its lifetime significantly. In contrast, LS-carbons with higher graphitic order display excellent structural stability but reduced capacitance due to limited accessible surface area and microporosity.

Therefore, optimal design requires moderate disorder of carbons with a hierarchical pore structure that combines micropores for capacitance and mesopores for ion transport. A gel electrolyte should have good conductivity and mechanical stability. This balance is key to simultaneously achieving high capacitance, energy efficiency, and long cycling stability.

Table S14 displays a summary of aqueous-gel based EC metrics. The idea of a lignin-based EC has already been proposed.[19,37] Park *et al.* reported an EC with an alkali lignin/PEGDGE-based GE containing 3.3 M KOH. Additionally, the authors prepared electrode carbon from alkali lignin/polyacrylonitrile with a relatively high S_{BET} value (1176 m^2 g^{-1}).[37] The gravimetric capacitance of the assembled EC was reported to be 129 F g^{-1} (0.5 A g^{-1}, 1 V); however, expensive gold current collectors were required.[37] On the other hand, Collins *et al.* reported an EC with an organosolv lignin/PEGDGE-based GE containing 6 M KOH and electrodes prepared through carbonization of a gel.[19] The gravimetric capacitance was 41 F g^{-1} (0.5 A g^{-1}, 1 V), but this work lacks details on carbon characterization, *e.g.*, S_{BET}.[19]

As a brief summary, these ECs use KOH-based non-practical aqueous electrolytes, and therefore, a higher voltage above 1.23 V cannot be applied, limiting their energy metrics, which are more affected by voltage than capacitance values ($E \sim U^2$). An in-depth comparison with these reported ECs is so difficult because different electrode materials and electrolytes were utilized as summarized in Table S14. Herein, the main strategy is to optimize the LSGE by using an aqueous acetate electrolyte with stable dielectric properties, which enables the EC to operate at a higher voltage of 1.6 V. Moreover, the salt templating approach was employed to reach the well-developed porosity of carbon as an electrode material. Owing to the optimization of EC lignosulfonate-based components, it was possible to reach both the high energetic metrics and long lifespan of LS-based ECs. It is worth underlining that our ECs were tested by floating at 1.6 V, which is harsh but very reliable for lifespan determination. Using cyclic voltammetry for long-term

testing[20] is not recommended, and hence galvanostatic cycling is adapted according to the international standards; however, floating is trustworthy especially in industries.

Additionally, in Table S14, we summarized the performance of ECs based on bio-derived gel electrolytes, which gives the idea of the capacitance values and lifespan of such systems. In particular, our LS-based EC outperforms the reported systems in terms of stable operating voltage and the majority of the capacitance values reported.[19,20,24,38] High capacitance values found in the literature could also be questionable, and the authors use a very small mass of electrode and/or often do not show the calculation procedure clearly.[20,38,98] The low conductivity of the gel type electrolyte is generally at the origin of moderate capacitance values.

Moreover, to further underline the green aspect of our work, we benchmarked our synthesis route against published LCAs for fossil- and lignin-based carbons. Conventional coal/oil-derived carbons exhibit a cradle-to-gate global warming potential of approximately 2.4 kg CO_2-eq per kg product.[99] In contrast, lignin-derived materials produced *via* similar slow-pyrolysis with subsequent heat treatment steps can achieve net-negative or near-neutral footprints, on the order of −0.23 kg CO_2 per kg product, with typical climate-change savings of 20–80% relative to fossil analogues.[100] Because our process uses a standard slow-pyrolysis heating rate (3 °C min^{-1}) followed by high-temperature, its energy demand is expected to be comparable to conventional carbon production, while the use of biogenic lignin and the potential for long-term carbon storage imply a substantially more favorable climate performance than coal-based carbons. Lignin, as a renewable material, participates in CO_2 removal from air through photosynthesis.[101] Regarding the environmental impact, CO_2 reduction by replacing fossil fuels with lignosulfonate-based EC components was estimated to range from 32% to 49%, as shown in Fig. S15. Compared with other references, our process is very promising for the further enhancement of environmental sustainability, ensuring good energy metrics of ECs.

4 Conclusions

For the first time, a gel electrolyte and porous carbon as the main components of ECs were synthesized from LS and optimized to enhance the sustainability of aqueous ECs with high performance. LS, a commercially available technical lignin, was selected as the dual precursor due to its environmental friendliness, high carbon content and water solubility. Moreover, the gel was composed of 72% LS, which is significantly better compared to other reported gels, making perfect use of the waste biopolymer.

The LS-based gel electrolyte was optimized using different liquid electrolytes through systematic investigation of its solution uptake ability, and 5 m KOAc was selected owing to the highest ion mobility for further application in ECs. The LS-carbon, prepared *via* a green salt templating approach, enabled precise control of the carbon structure and texture by selecting different template salts (NaOAc, KOAc, and their mixture NaKOAc). The amount and type of salt dictated the characteristics of carbon materials: (i) dominance of micropores, with a small fraction of mesopores for single salts (CLS-NaOAc and CLS-KOAc), (ii) high SSA ranging from 881 to 1754 m^2 g^{-1}, and (iii) various degrees of disorder (I_{D1}/I_G of 3.00–1.37), from highly disordered carbons (single salts) to ordered graphitized carbon (double salts).

The resultant EC assembled with an LS-based gel electrolyte and LS-carbons demonstrated a stable operating voltage of 1.6 V, a significant reduction in self-discharge (~30% loss of initial voltage), and a substantial lifespan of 170 h of floating. Hence, the performance of our LS-based EC is competitive with reference aqueous-based ECs. Moreover, the gel structure effectively inhibited electrolyte leakage, thereby enhancing the safety of the device. Nevertheless, using such a gel electrolyte eliminates the need for a separator, reducing the cost and environmental impact of the EC.

In summary, the valorization of water-soluble LS by its application as a precursor of the gel electrolyte and electrode material is an effective approach to reduce our dependence on non-renewable sources. It has been proven that LS waste can be transformed into valuable components of energy storage systems.

Author contributions

A. Klimek: conceptualization, data curation, formal analysis, investigation, methodology, visualization, writing – original draft, and writing – review & editing; L. Amro: investigation and writing – review & editing; N. Pakkang: investigation; C. Matei Ghimbeu: supervision, validation, and writing – review & editing; E. Frackowiak: conceptualization, funding acquisition, project administration, supervision, validation, and writing – review & editing; and S. Suzuki: conceptualization, funding acquisition, project administration, supervision, validation, and writing – review & editing.

Conflicts of interest

There are no conflicts of interest to declare.

Data availability

The data supporting this article have been included as part of the supplementary information (SI). Supplementary information is available. See DOI: https://doi.org/10.1039/d5gc05533d.

Acknowledgements

This research was supported by a French Government Scholarship France Excellence, Polish National Agency for Academic Exchange (NAWA) under the STER programme "Towards Internationalization of Poznan University of Technology Doctoral School (2022-2024)", the Ministry of Higher Education of Poland (Project 0911/SBAD/2501), the Japan Science and Technology Agency (JST) ALCA-Next (grant number: JPMJAN23C3), Co-Creation Core for Soft Materials Aspiring Research & Translation (C3-SMART), Japan Society for the Promotion of Science (JSPS) J-PEAKS and KAKENHI (grant number: 23H03828). The authors would like to acknowledge L. Vidal for the HRTEM analysis.

References

1 S. Wolf, R. Bullard, J. J. Buonocore, N. Donley, T. Farrelly, J. Fleming, D. J. X. Gonzalez, N. Oreskes, W. Ripple, R. Saha and M. D. Willis, *Oxf. Open Clim. Change*, 2025, **5**, 1–26.
2 G. Notton, M. L. Nivet, C. Voyant, C. Paoli, C. Darras, F. Motte and A. Fouilloy, *Renewable Sustainable Energy Rev.*, 2018, **87**, 96–105.
3 M. Zhou, A. Gallegos, K. Liu, S. Dai and J. Wu, *Carbon*, 2020, **157**, 147–152.
4 F. Béguin, V. Presser, A. Balducci and E. Frackowiak, *Adv. Mater.*, 2014, **26**, 2219–2251.
5 B. Dyatkin, V. Presser, M. Heon, M. R. Lukatskaya, M. Beidaghi and Y. Gogotsi, *ChemSusChem*, 2013, **6**, 2269–2280.
6 K. Dissanayake and D. Kularatna-Abeywardana, *J. Energy Storage*, 2024, **96**, 112563.
7 SkelCap, supercapacitor, Skeleton Technologies GmbH, preliminary data sheet, 2024.
8 J. Kowal, E. Avaroglu, F. Chamekh, A. Šenfelds, T. Thien, D. Wijaya and D. U. Sauer, *J. Power Sources*, 2011, **196**, 573–579.
9 S. Azmi, A. Klimek and E. Frackowiak, *Electrochim. Acta*, 2023, **452**, 142347.
10 K. Fic, A. Płatek, J. Piwek, J. Menzel, A. Ślesiński, P. Bujewska, P. Galek and E. Frąckowiak, *Energy Storage Mater.*, 2019, **22**, 1–14.
11 P. Galek, A. Slesinski, K. Fic and J. Menzel, *J. Mater. Chem. A*, 2021, **9**, 8644–8654.
12 M. Antonietti, N. Fechler and T. P. Fellinger, *Chem. Mater.*, 2014, **26**, 196–210.
13 A. Anukam, J. Berghel, G. Henrikson, S. Frodeson and M. Ståhl, *Renewable Sustainable Energy Rev.*, 2021, **148**, 111249.
14 C. Jaiswal, Lignosulfonate Market Size, Share & Industry Report 2034, Market Research Future, September 2025, https://www.marketresearchfuture.com/reports/lignosulfonate-market-26116.
15 J. Li, P. Yu, S. Zhang, Z. Wen, Y. Wen, W. Zhou, X. Dong, Y. Liu and Y. Liang, *J. Colloid Interface Sci.*, 2021, **600**, 586–593.
16 Y. K. Han, J. Y. Cheon, T. Kim, S. B. Lee, Y. D. Kim and B. M. Jung, *RSC Adv.*, 2020, **10**, 18945–18952.
17 F. Honda, S. Taira, S. Suzuki, K. Shikinaka, K. Shigetomi and Y. Uraki, *Holzforschung*, 2023, **77**, 776–783.
18 K. Gong, H. Lee, Y. Choi, G. Jung, K. Keum, J. W. Kim and J. S. Ha, *Electrochim. Acta*, 2024, **475**, 143585.
19 M. Muddasar, A. Beaucamp, M. Culebras and M. N. Collins, *Mater. Today Sustain.*, 2024, **26**, 100767.
20 G. Landi, L. La Notte, V. Granata, G. Avallone, C. Barone, G. Carapella, S. Pagano, A. L. Palma, P. Sdringola and G. Pugilisi, *ChemElectroChem*, 2023, **10**, e202300443.
21 Research Nester "Gel polymer electrolyte market" – size, emerging trends & forecast to 2035.
22 G. Wang, X. Lu, Y. Ling, T. Zhai, H. Wang, Y. Tong and Y. Li, *ACS Nano*, 2012, **6**, 10296–10302.
23 P. Yang, P. Zhang, C. Shi, L. Chen, J. Dai and J. Zhao, *J. Membr. Sci.*, 2015, **474**, 148–155.
24 S. Zallouz, J. M. L. Meins and C. Matei Ghimbeu, *Energy Adv.*, 2022, **1**, 1051–1064.
25 X. Hu, A. K. J. An and S. S. Chopra, *ACS Sustainable Chem. Eng.*, 2022, **10**, 5708–5718.
26 J. Huang, S. Wang, J. Chen, C. Chen and E. Lizundia, *Adv. Mater.*, 2025, **37**, 2416733.
27 F. Vollrath, R. Carter, G. K. Rajesh, G. Thalwitz and M. F. Astudillo "Life cycle analysis of cumulative energy demand on sericulture in Karnataka, India" BISERICA 2013 6th BACSA International Conference: Building Value Chains in Sericulture.
28 M. Lettner, P. Solt, B. Rößiger, D. Pufky-Heinrich, A. S. Jääskeläinen, P. Schwarzbauer and F. Hesser, *Sustainability*, 2018, **10**, 2745.
29 Borregaard USA, Inc., Environmental product declaration: sodium lignin biopolymer D powder, NEPD-5614-4920-EN, The Norwegian EPD Foundation, 2023.
30 T. Hammar, D. Peñaloza, A.-C. Hanning, N. Haatanen and J. Pakkasmaa, *J. Cleaner Prod.*, 2023, **426**, 139189.
31 J. Ding, Y. Yang, J. Poisson, Y. He, H. Zhang, Y. Zhang, Y. Bao, S. Chen, Y. M. Chen and K. Zhang, *ACS Energy Lett.*, 2024, **9**, 1803–1825.
32 A. Larrabide, I. Rey and E. Lizundia, *Adv. Energy Sustain. Res.*, 2022, **3**, 2200079.
33 A. Dér, N. Dilger, A. Kaluza, C. Creighton, S. Kara, R. Varley, C. Herrmann and S. Thiede, *J. Cleaner Prod.*, 2021, **303**, 127105.
34 G. Ma, M. Dong, K. Sun, E. Feng, H. Peng and Z. Lei, *J. Mater. Chem. A*, 2015, **3**, 4035–4041.
35 K. Subramani, N. Sudhan, R. Divya and M. Sathish, *RSC Adv.*, 2017, **7**, 6648–6659.
36 N. A. Choudhury, S. Sampath and A. K. Shukla, *Energy Environ. Sci.*, 2008, **2**, 55–67.
37 J. H. Park, H. H. Rana, J. Y. Lee and H. S. Park, *J. Mater. Chem. A*, 2019, **7**, 16962–16968.

38 H. F. Wan, X. Zhao, Q. Guo, C. Gao and R. C. Sun, *Front. Chem. Sci. Eng.*, 2025, **19**, 34.
39 S. Liu, R. Klukas, T. Porada, K. Furda, A. M. Fernández and A. Balducci, *J. Power Sources*, 2022, **541**, 231657.
40 J. Menzel, E. Frąckowiak and K. Fic, *Electrochim. Acta*, 2020, **332**, 135435.
41 Z. Zhang, J. Feng, Y. Jiang and J. Feng, *RSC Adv.*, 2017, **7**, 51096–51103.
42 C. Nita, M. Bensafia, C. Vaulot, L. Delmotte and C. Matei Ghimbeu, *Carbon*, 2016, **109**, 227–238.
43 A. Klimek, B. Réty, C. Matei Ghimbeu and E. Frackowiak, *Adv. Sci.*, 2025, **12**, e05032.
44 C. Decaux, C. Matei Ghimbeu, M. Dahbi, M. Anouti, D. Lemordant, F. Béguin, C. Vix-Guterl and E. Raymundo-Piñero, *J. Power Sources*, 2014, **263**, 130–140.
45 C. Nita, B. Zhang, J. Dentzer and C. Matei Ghimbeu, *J. Energy Chem.*, 2021, **58**, 207–218.
46 A. A. Ogale, M. Zhang and J. Jin, *J. Appl. Polym. Sci.*, 2016, **133**, 45.
47 M. Inagaki, Y. Hishiyama and Y. Kaburagi, *Carbon*, 1994, **32**, 637–639.
48 A. Sadezky, H. Muckenhuber, H. Grothe, R. Niessner and U. Pöschl, *Carbon*, 2005, **43**, 1731–1742.
49 S. Azmi, M. F. Koudahi and E. Frackowiak, *Energy Environ. Sci.*, 2022, **15**, 1156–1171.
50 M. Nishida, Y. Uraki and Y. Sano, *Bioresour. Technol.*, 2003, **88**, 81–83.
51 L. Passauer, K. Fischer and F. Liebner, *Holzforschung*, 2011, **65**, 309–317.
52 C. Marmorat, A. Arinstein, N. Koifman, Y. Talmon, E. Zussman and M. Rafailovich, *Nature*, 2016, **6**, 25495.
53 J. Aigoin, B. Bayre, J. M. Moncla, M. Escudero, D. Goudouneche, D. Ferri-Angulo, P. F. Calmon, L. Vaysse, P. Kemoun, L. Malaquin and J. Foncy, *ACS Omega*, 2025, **10**, 14687–14698.
54 B. Kumru, V. Molinari, M. Shalom, M. Antonietti and B. V. K. J. Schmidt, *Soft Matter*, 2018, **14**, 2655–2664.
55 S. D. Gong, Y. Huang, H. J. Cao, Y. H. Lin, Y. Li, S. H. Tang, M. S. Wang and X. Li, *J. Power Sources*, 2016, **307**, 624–633.
56 J. C. de Haro, E. Tatsi, L. Fagiolari, M. Bonomo, C. Barolo, S. Turri, F. Bella and G. Griffini, *ACS Sustainable Chem. Eng.*, 2021, **9**, 8550–8560.
57 M. Zhu, J. Wu, W.-H. Zhong, J. Lan, G. Sui and X. Yang, *Adv. Energy Mater.*, 2018, **8**, 1702561.
58 A. D. Drozdov and J. de Claville Christiansen, *Int. J. Solids Struct.*, 2017, **110–111**, 192–208.
59 S. Adapa and A. Malani, *Sci. Rep.*, 2022, **12**, 17810.
60 M. R. Lukatskaya, J. I. Feldblyum, D. G. Mackanic, F. Lissel, D. L. Michels, Y. Cui and Z. Bao, *Energy Environ. Sci.*, 2018, **11**, 2876–2883.
61 A. Alvarez-Coscojuela, J. Marco-Gibert, J. Mañosa, J. Formosa and J. M. Chimenos, *Appl. Clay Sci.*, 2024, **259**, 107515.
62 S. Azmi, A. Klimek and E. Frackowiak, *Mater. Today*, 2023, **68**, 34–50.
63 A. Laheäär, P. Przygocki, Q. Abbas and F. Béguin, *Electrochem. Commun.*, 2015, **60**, 21–25.
64 S. Zallouz, L. Dentzer and C. Matei Ghimbeu, *ACS Appl. Energy Mater.*, 2024, **7**, 1448–1460.
65 A. C. Ferrari and J. Robertson, *Phys. Rev. B: Condens. Matter Mater. Phys.*, 2000, **61**, 14095–14107.
66 Z. Li, L. Deng, I. A. Kinloch and R. J. Young, *Prog. Mater. Sci.*, 2023, **135**, 101089.
67 S. Biniak, M. Pakuła, A. Świątkowski, M. Bystrzejewski and S. Błażewicz, *J. Mater. Res.*, 2010, **25**, 1617–1628.
68 F. Tuinstra and J. L. Koenig, *J. Chem. Phys.*, 1970, **53**, 1126–1130.
69 A. Platek-Mielczarek, C. Nita, C. Matei Ghimbeu, E. Frackowiak and K. Fic, *ACS Appl. Mater. Interfaces*, 2021, **13**, 2584–2599.
70 M. Thommes, K. Kaneko, A. V. Neimark, J. P. Olivier, F. Rodriguez-Reinoso, J. Rouquerol and K. S. W. Sing, *Pure Appl. Chem.*, 2015, **87**, 1051–1069.
71 Q. Abbas, D. Pajak, E. Frąckowiak and F. Béguin, *Electrochim. Acta*, 2014, **140**, 132–138.
72 F. Salvador, C. Sánchez-Jiménez, M. J. Sánchez-Montero and A. Salvador, in *Studies in Surface Science and Catalysis*, ed. F. Rodriguez-Reinoso, B. McEnaney, J. Rouquerol and K. Unger, Elsevier, 2002, vol. 144, pp. 379–386.
73 J. Jagiello and J. P. Olivier, *Carbon*, 2013, **55**, 70–80.
74 S. Porada, L. Borchardt, M. Oschatz, M. Bryjak, J. S. Atchison, K. J. Keesman, S. Kaskel, P. M. Biesheuvel and V. Presser, *Energy Environ. Sci.*, 2013, **6**, 3700–3712.
75 A. Adeniji, A. Beda, P. Fioux and C. Matei Ghimbeu, *J. Mater. Chem. A*, 2025, **13**, 14896–14914.
76 Y. J. Heo and S. J. Park, *Energy*, 2015, **91**, 142–150.
77 M. G. Plaza, A. S. González, J. J. Pis, F. Rubiera and C. Pevida, *Appl. Energy*, 2014, **114**, 551–562.
78 J. Ludwinowicz and M. Jaroniec, *Carbon*, 2015, **82**, 297–303.
79 N. Díez, A. B. Fuertes and M. Sevilla, *Energy Storage Mater.*, 2021, **38**, 50–69.
80 L. Cheng, K. Zhang, Q. Nie, G. Wang, X. Cai, M. Zhang, C. Liu and Z. Shen, *Energy Fuels*, 2023, **37**, 13405–13414.
81 J. Dai, S. Tian, Y. Jiang, Z. Chang, A. Xie, R. Zhang and Y. Yan, *J. Alloys Compd.*, 2018, **732**, 222–232.
82 P. L. Taberna and P. Simon, *Supercapacitors*, John Wiley & Sons, Ltd, 2013, pp. 111–130.
83 A. Parejo-Tovar and F. Béguin, *Energy Storage Mater.*, 2024, **69**, 103387.
84 B. E. Conway, in *Electrochemical Supercapacitors*, Springer US, Boston, MA, 1999, pp. 525–556.
85 K. B. Li, D. W. Shi, Z. Y. Cai, G. L. Zhang, Q. A. Huang, D. Liu and C. P. Yang, *Electrochim. Acta*, 2015, **174**, 596–600.
86 D. Bresser, D. Buchholz, A. Moretti, A. Varzi and S. Passerini, *Energy Environ. Sci.*, 2018, **11**, 3096–3127.
87 M. Rajkumar, C.-T. Hsu, T. H. Wu, M. G. Chen and C. C. Hu, *Prog. Nat. Sci.:Mater. Int.*, 2015, **25**, 527–544.
88 D. Jain, J. Kanungo and S. K. Tripathi, *Mater. Chem. Phys.*, 2019, **229**, 66–77.

89 Y. R. Hu, X. L. Dong, H. K. Zhuang, D. Yan, L. Hou and W. C. Li, *ChemElectroChem*, 2021, **8**, 3073–3079.
90 A. Lewandowski, P. Jakobczyk, M. Galinski and M. Biegun, *Phys. Chem. Chem. Phys.*, 2013, **15**, 8692–8699.
91 J. Niu, B. E. Conway and W. G. Pell, *J. Power Sources*, 2004, **135**, 332–343.
92 A. Beda, C. Vaulot, F. Rabuel, M. Morcrette and C. Matei Ghimbeu, *Energy Adv.*, 2022, **1**, 185–190.
93 X. Liu, D. Lyu, C. Merlet, M. J. A. Leesmith, X. Hua, Z. Xu, C. P. Grey and A. C. Forse, *Science*, 2024, **384**, 321–325.
94 P. Ratajczak, K. Jurewicz and F. Béguin, *J. Appl. Electrochem.*, 2014, **44**, 475–480.
95 S. E. M. Pourhosseini, A. Bothe, A. Balducci, F. Beguin and P. Ratajczak, *Energy Storage Mater.*, 2021, **38**, 17–29.
96 E. Pamete, L. Kops, F. A. Kreth, S. Pohlmann, A. Varzi, T. Brousse, A. Balducci and V. Presser, *Adv. Energy Mater.*, 2023, **13**, 2301008.
97 M. He, K. Fic, E. Frąckowiak, P. Novák and E. J. Berg, *Energy Environ. Sci.*, 2016, **9**, 623–633.
98 J. Wang, C. Gao, P. Hou, Y. Liu, J. Zhao and P. Huo, *Chem. Eng. J.*, 2023, **455**, 140952.
99 D. Maga, V. Aryan and J. Blömer, *Resour., Conserv. Recycl.*, 2023, **199**, 107255.
100 Z. N. Akhlisah, H. C. Ong, H. V. Lee and Y. H. Tan, *Renewable Sustainable Energy Rev.*, 2026, **226**, 116363.
101 C. Moretti, B. Corona, R. Hoefnagels, I. Vural-Gürsel, R. Gosselink and M. Junginger, *Sci. Total Environ.*, 2021, **770**, 144656.